

# Aging-associated HELIOS deficiency in naive CD4<sup>+</sup> T cells alters chromatin remodeling and promotes effector cell responses

Received: 15 January 2022

Accepted: 24 October 2022

Published online: 12 December 2022

 Check for updates

Huimin Zhang<sup>1,2,7</sup>, Rohit R. Jadhav<sup>1,2,7</sup>, Wenqiang Cao<sup>1,2,3</sup>, Isabel N. Goronzy<sup>4</sup>, Tuantuan V. Zhao<sup>2,5</sup>, Jun Jin<sup>1,2</sup>, Shozo Ohtsuki<sup>2,5</sup>, Zhaolan Hu<sup>2,5</sup>, Jose Morales<sup>5</sup>, William J. Greenleaf<sup>6</sup>, Cornelia M. Weyand<sup>1,2,5</sup> & Jörg J. Goronzy<sup>1,2,5</sup> ✉

Immune aging combines cellular defects in adaptive immunity with the activation of pathways causing a low-inflammatory state. Here we examined the influence of age on the kinetic changes in the epigenomic and transcriptional landscape induced by T cell receptor (TCR) stimulation in naive CD4<sup>+</sup> T cells. Despite attenuated TCR signaling in older adults, TCR activation accelerated remodeling of the epigenome and induced transcription factor networks favoring effector cell differentiation. We identified increased phosphorylation of STAT5, at least in part due to aberrant IL-2 receptor and lower HELIOS expression, as upstream regulators. Human HELIOS-deficient, naive CD4<sup>+</sup> T cells, when transferred into human-synovium-mouse chimeras, infiltrated tissues more efficiently. Inhibition of IL-2 or STAT5 activity in T cell responses of older adults restored the epigenetic response pattern to the one seen in young adults. In summary, reduced HELIOS expression in non-regulatory naive CD4<sup>+</sup> T cells in older adults directs T cell fate decisions toward inflammatory effector cells that infiltrate tissue.

Aging is associated with impaired immune function that manifests as an increased susceptibility to infections drastically highlighted in the current pandemic of SARS-CoV-2 (refs. <sup>1,2</sup>). Vaccination efficacy in the senior population against many pathogens is attenuated<sup>3,4</sup>, stressing the relevance of the aging of CD4<sup>+</sup> T cells, the major orchestrator of the response to most current vaccines. Defects in adaptive immunity coexist with or may even contribute to the activation of inflammatory pathways in older adults, also called inflamm-aging<sup>5</sup>. Simplified models, such as a decline in the total number of naive T cells or contraction of TCR diversity due to reduced thymic activity are insufficient to explain age-associated immune dysfunction<sup>6,7</sup>. In fact, while the frequency of

naive CD4<sup>+</sup> T cells declines with age and their TCR richness is reduced, the pool of naive CD4<sup>+</sup> T cells in human older adults is still large<sup>8</sup> and diverse<sup>9</sup>. Although age-associated defects in TCR signaling have been described in many studies<sup>10–12</sup>, naive CD4<sup>+</sup> T cells from older human adults have been found to display a bias to differentiate into effector T cells upon activation<sup>13</sup>. The mechanisms overcoming the defective signaling and driving excessive effector cell differentiation are unresolved, but may include an epigenetic primed state<sup>14</sup>. Such an epigenetic predisposition could explain the higher frequency of effector T cell populations with age<sup>15</sup> that contribute to the increased production of inflammatory mediators.

<sup>1</sup>Department of Immunology, Mayo Clinic, Rochester, MN, USA. <sup>2</sup>Department of Medicine, Stanford University, Stanford, CA, USA. <sup>3</sup>Health Sciences Institute, China Medical University, Shenyang, China. <sup>4</sup>Biochemistry and Molecular Biophysics, California Institute of Technology, Pasadena, CA, USA. <sup>5</sup>Department of Medicine, Division of Rheumatology, Mayo Clinic, Rochester, MN, USA. <sup>6</sup>Department of Genetics, Stanford University, Palo Alto, Stanford, CA, USA. <sup>7</sup>These authors contributed equally: Huimin Zhang, Rohit R. Jadhav. ✉e-mail: [goronzy.jorg@mayo.edu](mailto:goronzy.jorg@mayo.edu)

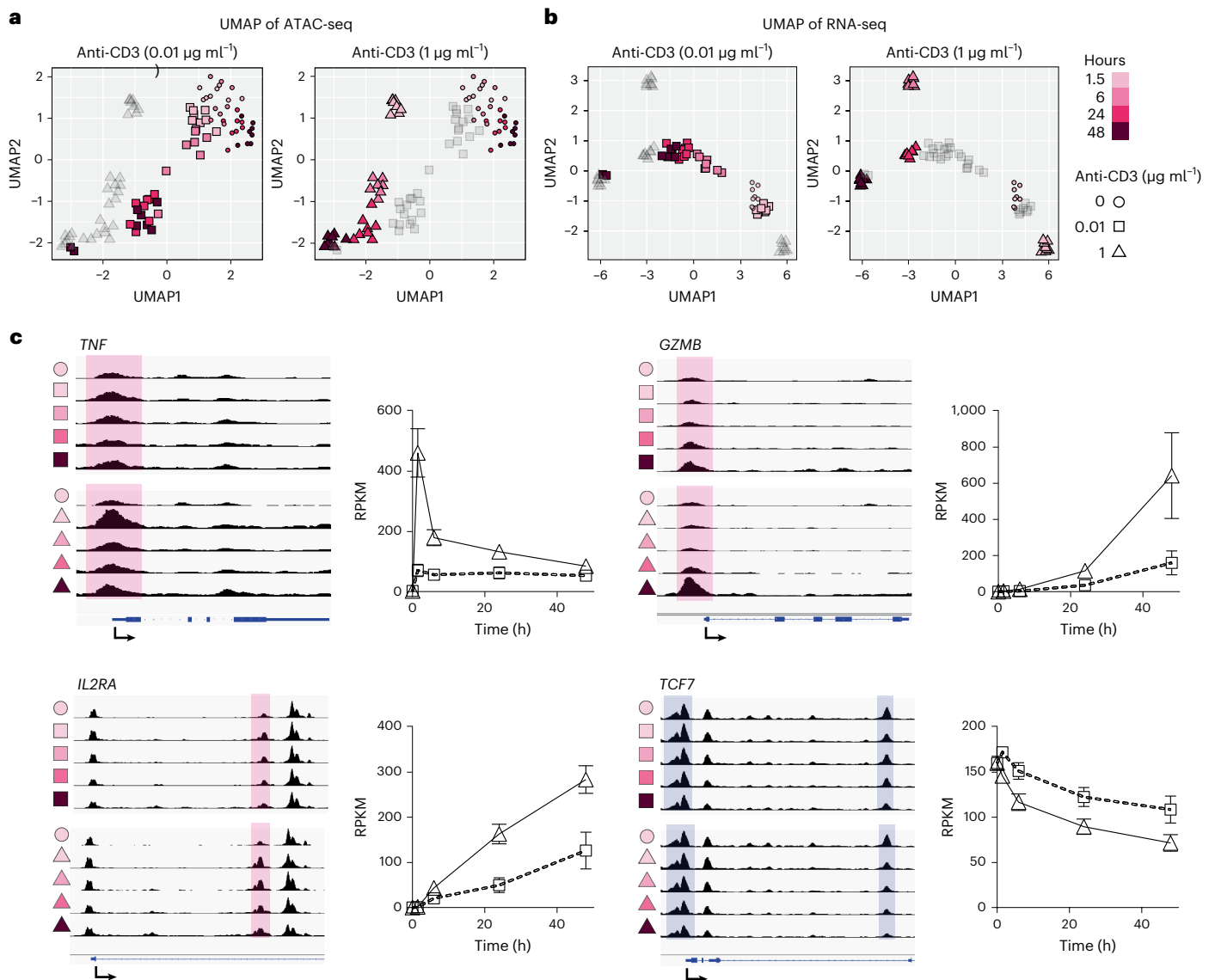


**Fig. 1 | Chromatin accessibility changes induced by TCR stimulation of different signaling strengths. a**, ATAC-seq UMAP visualization of naive  $\text{CD4}^+$  T cells from eight healthy individuals stimulated with 0.01  $\mu\text{g ml}^{-1}$  (squares) and 1  $\mu\text{g ml}^{-1}$  anti-CD3-coated beads (triangles) for 1.5, 6, 24 or 48 h. Time points are indicated by color code. Samples stimulated with 0  $\mu\text{g ml}^{-1}$  anti-CD3-coated beads were included as control (circles). Peaks changing in accessibility after low- or medium-intensity TCR stimulation were identified as described in Extended Data Fig. 2b. **b**, RNA-seq UMAP visualization of the same set of

samples. Differentially expressed transcripts were identified as described in Extended Data Fig. 2d. **c**, Aggregate genome tracks that close or open with TCR stimulation. Color codes indicating time points and symbols defining anti-CD3 concentrations are as defined in **a** and **b**. Red-shaded areas indicate peaks that open with TCR stimulation and blue areas indicate peaks that close. Corresponding gene expression data are shown as mean  $\pm$  s.e.m. (right).  $n = 8$  biologically independent samples. RPKM, reads per kilobase of exon per million reads mapped.

System approaches integrating the different dimensions of functional pathways are needed to determine how age affects immune responses and to identify targets of interventions. Excellent work has been done in the murine system, including recent profiling of the aged immune system at single-cell resolution<sup>15–17</sup>; however, T cell homeostasis over a lifetime is fundamentally different in mice and humans<sup>18</sup>, and age-associated changes in T cell population composition and cell function are therefore influenced by species differences<sup>19</sup>. Only one of these omics studies have examined whether the findings are relevant for human immune aging<sup>17</sup>. Moreover, static cross-sectional studies are only the first step and need to be followed by dynamic studies to identify the causality between age-associated changes. While such studies are more feasible in the mouse<sup>20,21</sup>, they may not always reflect the human system.

Here we monitored the trajectory of epigenetic and transcriptional changes of naive  $\text{CD4}^+$  T cells from young and older adults after TCR stimulation, aiming to capture aging signatures falling into the early kinetic window. We observed that naive  $\text{CD4}^+$  T cells from healthy older individuals had a higher propensity to TCR activation-induced chromatin changes despite having reduced phosphorylation of signaling molecules. Analysis of kinetic changes identified STAT5 as the candidate upstream transcription factor (TF) driving excess TCR-induced differentiation exemplified by higher IRF4, BATF and BLIMP1 expression. Single-cell multiome (scMultiome) profiling of naive  $\text{CD4}^+$  T cells activated for 18 h, integrating chromatin accessibility and transcriptomic data, revealed a subpopulation enriched for STAT5 activity that was increased in frequency with age. This early STAT5 activity was caused by the early upregulation of CD25 on naive T cells due to a loss of the

TF HELIOS. Pharmacological degradation of HELIOS in naive CD4<sup>+</sup> T cells favored effector T cell differentiation and tissue infiltration in a human mouse chimera model. Inhibiting STAT5 signaling reoriented the epigenetic landscape of naive CD4<sup>+</sup> T cells in older individuals and dampened the proinflammatory effector cell formation by reducing BLIMP1 expression and increasing TCF1.

## Results

### Epigenomic remodeling in activated naive CD4<sup>+</sup> T cells

Studies on the activation of human T cells have to rely on in vitro polyclonal stimuli that are generally supra-physiological and may therefore mask functionally important differences. To mimic TCR signal inputs in the more physiological range, we stimulated T cells with polystyrene beads that had been coated with increasing amounts of anti-CD3 and a constant amount of anti-CD28. The density of anti-CD3 on these beads was multifold lower than the commercial Dynabeads. Anti-CD28 concentrations were chosen to optimize formation of cell–bead conjugates irrespective of anti-CD3 levels (Extended Data Fig. 1a). Phosphorylation of signaling molecules was determined on gated cells attached to beads to control for any difference in conjugate formation. As shown for phosphorylated ERK, stimulation with both low and high anti-CD3 concentrations resulted in the activation of the entire conjugate population, with populations shifting by different degrees (Extended Data Fig. 1b). Early signaling as represented by ZAP70 and SLP76 phosphorylation and downstream signaling events as represented by ERK phosphorylation correlated with anti-CD3 levels on the beads (Extended Data Fig. 1c). Anti-CD3 concentrations of 0.01  $\mu\text{g ml}^{-1}$ , which induced half-maximal ERK phosphorylation, and 1  $\mu\text{g ml}^{-1}$ , at which ERK phosphorylation plateaued, were used in subsequent experiments as low and medium TCR signal inputs, respectively. The selected range of TCR signaling strengths was very effective in inducing CD69 expression as seen by similar kinetics and intensity of CD69 in cells bound to beads (Extended Data Fig. 1d).

To examine epigenomic and transcriptional changes, we stimulated naive CD4<sup>+</sup> T cells from healthy individuals with anti-CD3/anti-CD28-coated beads and performed ATAC-seq and RNA-seq at four time points over 48 h before any cell division had occurred (Extended Data Fig. 1e). Results at no, low and medium TCR signal input (0, 0.01 and 1  $\mu\text{g ml}^{-1}$  anti-CD3) are shown as Uniform Manifold Approximation and Projection (UMAP) plots. The samples clustered according to anti-CD3 concentration and post-activation time (Fig. 1a,b). Data from cells cultured with only anti-CD28 showed low variability without time-dependent directionality in chromatin changes. Clustering at different time points after low-grade stimulation was not very clear due to high inter-individual heterogeneity. Changes in chromatin accessibilities were minimal in the first 6 h; most changes occurred between 6 and 24 h. In contrast, a major shift was seen in UMAP1 within 1 h of higher intensity stimulation followed by a shift in UMAP2 over the next 24 to 48 h (Fig. 1a). The patterns were similar for transcriptome data (Fig. 1b).

To gain insights on the TCR stimulation-induced epigenomic changes, we identified differentially opened chromatin sites between TCR-stimulated T cells and those without stimulation across the entire

time course. The number of differentially open sites increased over time (Extended Data Fig. 2a). Cumulatively, about 5,000 sites changed in accessibility in response to low and 30,000 sites to medium TCR signal (Extended Data Fig. 2b). Correspondingly, about 2,000 genes were differentially expressed in response to the low and 6,000 genes to the medium signal (Extended Data Fig. 2c,d). Typical activation-associated genes such as *TNF*, *IL2RA* and *GZMB* gained chromatin accessibility after TCR stimulation and quiescence-associated genes such as *TCF7* lost accessibility (Fig. 1c). Transcript expression closely trailed changes in chromatin accessibility (Fig. 1c). Taken together, the differential TCR signal inputs induced dynamic and signal strength-dependent chromatin accessibility changes in naive CD4<sup>+</sup> T cells.

### Chromatin accessibility responses are higher in older adults

TCR signaling has been shown to be blunted with age, in part due to a reduced expression of miR-181a and the associated increased concentrations of several phosphatases<sup>10,11</sup>. Consistent with these studies, we found reduced ERK and LAT phosphorylation in naive CD4<sup>+</sup> T cells from older individuals stimulated with 1  $\mu\text{g ml}^{-1}$  anti-CD3/CD28-coated beads (Fig. 2a,b). We therefore expected activation-induced epigenomic changes in T cells from older individuals to be shifted to those seen with lower signaling strength in young adults. Our study population shown in Fig. 1 included four 21–35-year-old adults and four adults older than 65 years (Supplementary Table 1). To identify age-dependent shifts in the activation-induced epigenetic state of naive CD4<sup>+</sup> T cells, we performed principal-component analysis (PCA) of the 5,000 most variable sites and plotted the result separately for samples from young and older individuals across the 48-h time course. Results are shown for PC1, which explained 50% of the variance (Fig. 2c), whereas other PCs accounted for less than 8% of variance each. For cells cultured with beads lacking anti-CD3, both young and older individuals had no clear kinetic changes along the time course. At low TCR input, all individuals showed an increase in PC1 starting from 6 h of stimulation while at medium TCR input, the increase started as early as at 1.5 h (Fig. 2c). Notably, older individuals maintained at least an equal PC1 score at both TCR signal inputs compared to those from young adults. This contrasts with the blunted TCR signaling, suggesting that the activation-induced chromatin state and early signaling events are uncoupled with age.

Cumulatively over the time course after activation with higher intensity stimulation, 3,078 sites had higher and 2,557 lower accessibility in T cells from older compared to young adults. Largely, these peaks included sites that were differentially accessible at lower stimulation (Extended Data Fig. 3). In our subsequent analysis, we therefore focused on the dataset from higher intensity stimulation.

We sought to first determine whether the response in older individuals had unique kinetic features. We used fuzzy *c*-means clustering on all sites that had changed with stimulation to identify temporal patterns of activation-induced chromatin changes in each age group. Seven clusters (from a range of 2 to 10) were chosen as the minimal number capturing different patterns. In Fig. 2d, clusters are ordered by the emergence of early changes in the time course. Six clusters were largely similar between the two age groups, with small kinetic differences,

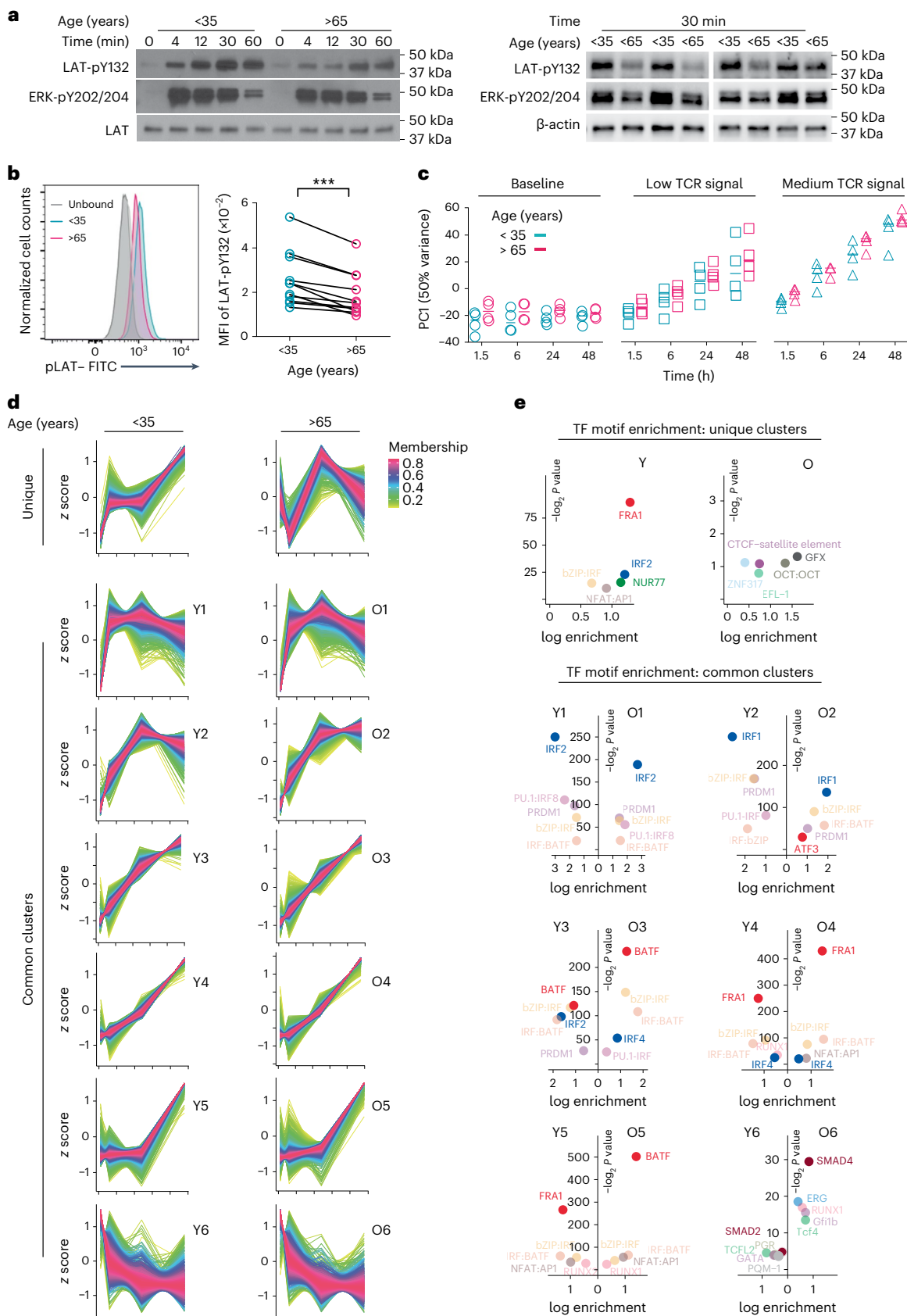
### Fig. 2 | Dissociation of TCR-induced signaling and chromatin accessibility changes in naive CD4<sup>+</sup> T cells from older adults. a, LAT and ERK phosphorylation was measured from 0 to 60 min after stimulation of naive CD4<sup>+</sup> T cells with polystyrene beads coated with 1 $\mu\text{g ml}^{-1}$ anti-CD3 (left).

Phosphorylation at 30 min was measured for four young and four older individuals (right). b, Representative histograms of phosphorylated LAT of unbound cells (gray lines) or bead–cell conjugates (magenta and cyan lines) measured by flow cytometry (left). Mean fluorescence intensity (MFI) of phosphorylated LAT of naive CD4<sup>+</sup> T cells from 11 young and 11 older individuals; data from 11 experiments. Data were analyzed with two-sided paired Student's *t*-test;  $P = 0.0002$ . c, PCA was performed on the 5,000 most variable sites of the ATAC-seq dataset described in Fig. 1a. PC1, accounting for 50% variance, is shown separately for stimulated naive CD4<sup>+</sup> T cells from young and older adults.  $n = 8$

biologically independent samples. d, Peak sets from ATAC-seq data of young and older adults were generated that significantly differed from baseline at any of the post-stimulation time points. Peaks from younger and older adults were separately subjected to TCseq clustering. Results are shown for seven clusters with different temporal patterns, six of them grossly similar between young and old. Membership scores, representing the likelihood of a peak to be in this cluster, are indicated by color code. e, Peak sets with membership scores >0.6 were analyzed for TF motif enrichments by HOMER. Graphs show the fold enrichment (*x* axis) in each cluster from young (left) and old (right) adults plotted versus the significance level (*y* axis). Comparisons were conducted by two-sided robust empirical Bayes moderated statistical test; a Benjamini–Hochberg adjusted *P* value of 0.001 was used as a cutoff. The five TFs with the lowest *P* values are named.

suggesting that the progression of chromatin changes after T cell activation was not grossly influenced by age. Clustering correlated with enrichment for selective TFs (Fig. 2e). A cluster unique for young adults

displayed an early rapid change followed by a plateau for 24 h before further differentiation. Biological pathway analysis showed that the annotated genes of this cluster were enriched for the T cell activation



pathway (Extended Data Fig. 4a); TF motif enrichment analysis suggested regulation by FRA1, nuclear factor (NF)- $\kappa$ B and NUR77 (Fig. 2e), consistent with the increased TCR signaling in young adults. The unique cluster in older adults did not show significant enrichment of any TF motif (Fig. 2e). Clusters 1 and 2, next in the time course, were enriched for IRF family member motifs. Sites in clusters 3–5 were progressively opening over the entire 48 h. Corresponding genes were enriched for developmental pathways (Extended Data Fig. 4a). Motif analysis suggested bZIP family members as the dominant upstream regulators (Fig. 2e). Transcript analysis supported the regulation of temporal patterns by different TFs as implicated by motif enrichment (Extended Data Fig. 4b). *NR4A1* (encoding NUR77) peaked early, followed by *IRF1* and *IRF4*. bZIP family TFs came in several waves. *FRA1* was rapidly induced in the first hour, whereas *BATF* was progressively upregulated throughout the 48-h time course (Extended Data Fig. 4b). Notably, clusters 3–5 all showed higher enrichment for bZIP family motifs in T cells from older adults (Fig. 2e), consistent with an elevated transcription of *BATF* in older adults (Extended Data Fig. 4b). A similar pattern was observed for *BLIMP1* encoded by *PRDM1* (Extended Data Fig. 4b). Sites of cluster 6, closing immediately after TCR stimulation, were regulated by SMAD family members and enriched for T cell activation and adhesion pathways. Collectively, our data suggest that despite blunted TCR signaling, T cells from older adults exhibited a similar temporal pattern in TCR stimulation-induced chromatin changes and even an excess in accessibility to the bZIP family members at later time points.

### Higher chromatin changes in older adults are driven by STAT5

The propensity of T cells from older adults to undergo accelerated TCR-induced chromatin changes cannot be explained by TCR signaling that is even blunted (Fig. 2a,b). To identify alternative potential upstream regulators that preceded the increased accessibility to bZIP family motifs, we identified enriched TF-binding motifs in the whole peak set using ChromVAR. TFs with deviation score differences in the top ten percentile were plotted separately for young and older individuals (Fig. 3a). The TF clustering patterns fell into two categories: one with TF-binding sites closing across the time course (for example, the ETS family), and one with TF-binding sites opening (for example, the STAT, IRF and bZIP families). These later TFs trended to show higher deviation scores in older individuals (Fig. 3a). STAT5 motif enrichment plateaued as early as at 6 h, IRF4 at 24 h, whereas *BATF* was still rising at 48 h (Fig. 3b). These data suggest that STAT5 may be the primary TF that drives elevated activation-induced chromatin changes in older adults.

To corroborate our findings from ChromVAR, we identified peaks differentially accessible between young and older individuals at each time point (Extended Data Fig. 5a) and performed *k*-means clustering. Gap statistics suggested clustering into ten groups (Fig. 3c). Accessibility tracks of genes representative for each cluster are shown together with the corresponding transcript data (Fig. 3d and Extended Data Fig. 5b). Accessibility differences at each of the time points correlated with the fold difference in transcripts at 48 h (Extended Data Fig. 5c). Most of

the closing sites (clusters 7–10) were already different at baseline and regulated by members of the ETS family, suggesting that these aging signatures are imprinted at the quiescent state. In contrast, increased accessibility in older individuals was generally activation-induced, and sites were enriched for STAT, bZIP and bZIP:IRF family motifs (clusters 2–5). Only sites opening after activation in cluster 1, enriched for TCF motifs, were less accessible in older adults.

To validate the sequence of increased TF activities in older adults, we examined the protein level of implicated TFs. Consistent with the temporal pattern in ChromVAR, phosphorylated STAT5 (pSTAT5) emerged early followed by IRF4 and *BATF* (Fig. 3e). In CD4<sup>+</sup> T cell responses from older individuals, pSTAT5 peaked already at 6 h when it displayed minimal activity in younger adults ( $P < 0.01$ ). After 24 h of stimulation, expression of IRF4 and *BATF* was higher in the older adults ( $P < 0.01$ ; Fig. 3f,g). A STAT5 inhibitor reduced upregulation of IRF4 and *BATF* expression at 9–24 h after activation (Fig. 3h and Extended Data Fig. 6), corroborating that pSTAT5 drives the accelerated chromatin changes in naive CD4<sup>+</sup> T cells from older adults.

### CD4<sup>+</sup> T cells with increased STAT5 activity in older adults

The increased epigenetic TCR response may reflect a distinct subset that increases with age<sup>22</sup>. Naive CD4<sup>+</sup> T cells include a CD31<sup>+</sup>PTK7<sup>+</sup> population of recent thymic emigrants that declines with age (Extended Data Fig. 7a); however, this population is too small to account for the observation. To investigate population heterogeneity, we employed scMultiomics (combined scRNA-seq and ATAC-seq). The cluster of 18-h TCR-stimulated naive CD4<sup>+</sup> T cells was distinctly separate from resting cells in UMAP plots and characterized by *CD69* expression (Extended Data Fig. 7a). Within activated cells, four subclusters were distinguished, most obviously, when ATAC-seq and RNA-seq data were integrated (Fig. 4a). TF-binding motif analysis revealed that cluster 1 was enriched for KLF4-binding, clusters 1 and 2 for STAT5-binding and clusters 3 and 4 for BACH2-binding and NFAT-binding accessible sites (Fig. 4b). TF-binding footprints confirmed increased pSTAT5 activity in cluster 2, BACH2 in clusters 3 and 4 and NFAT in cluster 4. Clusters were also distinct in their transcriptomes. Cluster 1 did not exhibit the downregulation of *CXCR4* seen after T cell activation in bulk RNA-seq data. Pathway analysis showed that cluster 1 was enriched in senescence-associated and T cell activation-resistant genes, suggesting that cluster 1 contained low responding cells. Cluster 2 showed high transcript numbers of *PRDM1* and was enriched for RUNX3-regulated immune responses, reflective of effector precursors. Cluster 3 was enriched for TCF1 and BACH2 targets, both of which are involved in the differentiation of memory precursors. Cluster 4 showed high expression of *CD69*, *TNF* and *IL2*, all of which are signs of T cell activation, and thus was referred to as fast responders (Fig. 4b).

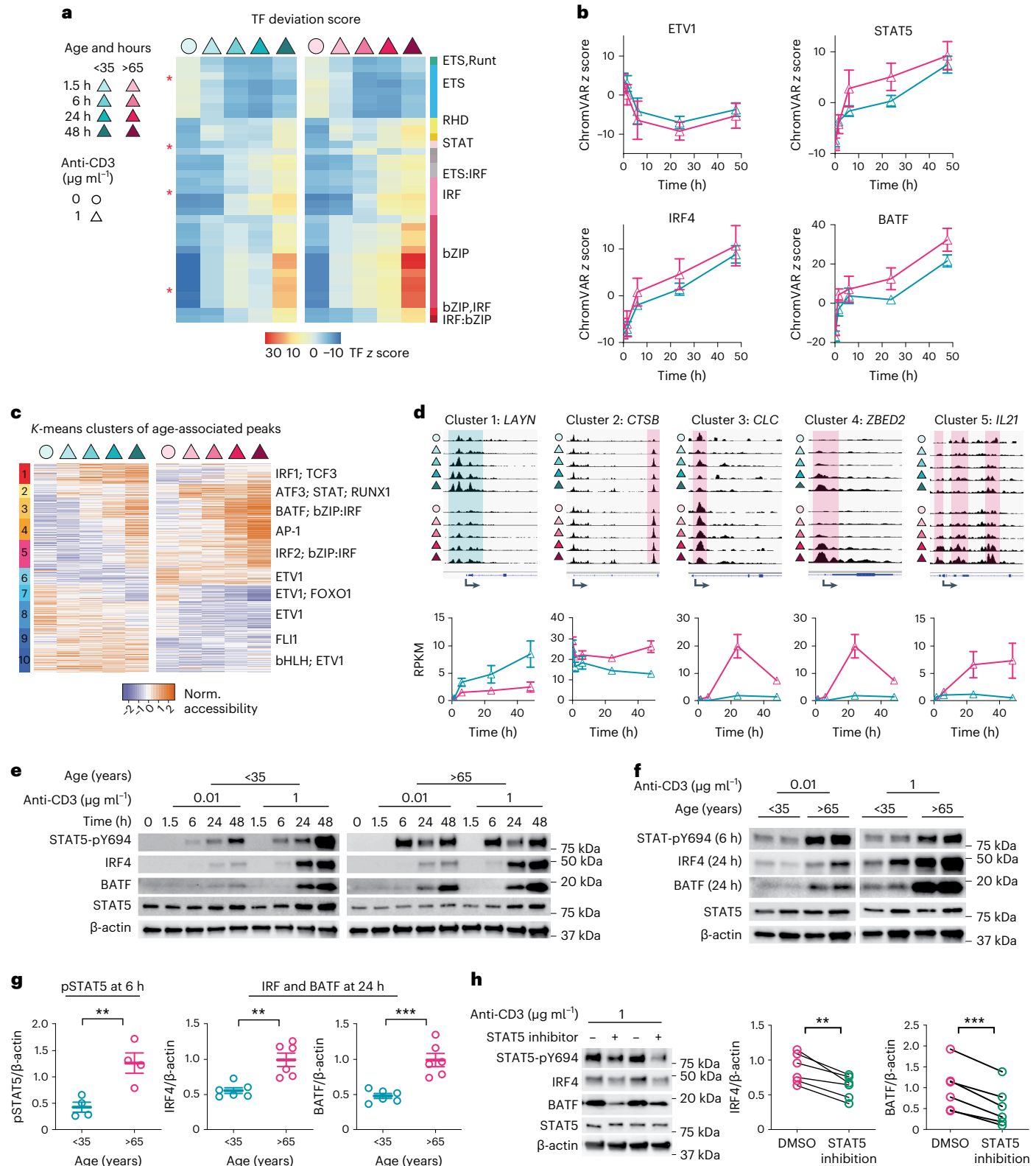
To explore whether the excess in activation-induced chromatin modifications in older adults was representative of the whole naive CD4<sup>+</sup> T cell compartment or reflected distinct subpopulations, we plotted UMAPs of activated single cells of younger and older individuals

**Fig. 3 | Accelerated chromatin changes in T cells from older adults are driven by the STAT5 pathway.** **a**, Heat map representation of top 35 most variable TFs based on ChromVAR deviation scores of the ATAC-seq data described in Fig. 1a. Each column is the score median of four younger and four older individuals. **b**, ChromVAR deviation scores for representative TFs indicated by stars in **a** are shown as mean + s.e.m.  $n = 8$  biologically independent samples. **c**, *K*-means clustering of peaks differentially accessible between younger and older individuals at any time point after medium-intensity TCR stimulation (Extended Data Fig. 5a). TFs with the highest binding motif enrichment for each cluster are indicated. **d**, Aggregate genome tracks of representative sites of clusters 1–5 in **c** (top). Magenta-shaded areas indicate peaks that open more in older adults; peaks that are open more in younger adults are shaded cyan. Gene expression from RNA-seq data (bottom) shown as mean + s.e.m.  $n = 8$  biologically independent samples. **e**, Phosphorylated STAT5 (pSTAT5), IRF4 and *BATF* were

measured at indicated times after TCR stimulation. Immunoblots are shown for one young and one older individual representative of three experiments. **f**, Representative blots of pSTAT5 measured at 6 h and IRF4 and *BATF* at 24 h after low and median intensity stimulation. **g**, Summary results for 4–6 younger and 4–6 older adults measured in four experiments; median intensity stimulation shown as mean  $\pm$  s.e.m. (bottom).  $n = 12$  biologically independent samples. Data were analyzed with two-sided unpaired Student's *t*-test.  $**P < 0.01$  ( $P = 0.008$  for pSTAT5 and  $P = 0.002$  for IRF4);  $***P < 0.001$  ( $P = 0.0005$ ). **h**, Naive CD4<sup>+</sup> T cells from older adults were activated for 48 h with indicated anti-CD3-coated beads in the presence of DMSO control or a STAT5 inhibitor. Representative blots for pSTAT5, IRF4 and *BATF* (left). Summary results of three experiments (right).  $n = 6$  biologically independent samples. Data were analyzed with two-sided paired Student's *t*-test.  $**P < 0.01$  ( $P = 0.0035$ ),  $***P < 0.001$  ( $P = 0.0004$ ).

separately (Fig. 4c). Older individuals had notably larger effector precursor and low-responder clusters, both enriched for accessibility to STAT5 binding sites (Fig. 4b,c). Moreover, cells from older adults in cluster 2 exhibited increased expression of CD25 and of several TFs involved in T effector cell differentiation (for example, *IRF4*, *PRDM1*, *BHLHE40* and *MAF*) (Fig. 4d). The memory precursor cluster, enriched for BACH2-binding sites, was smaller in older individuals (Fig. 4b,c)

and *BACH2* expression was lower in activated CD4<sup>+</sup> T cells from older adults (Fig. 4e). The lower expression of *BACH2* in older adults could render T cells from older adults more susceptible to activation<sup>23,24</sup> and may contribute to the accelerated accessibility to bZIP motifs as shown in Fig. 2d. Similarly, expression of *MYC* was largely limited to clusters 3 and 4 and was increased in T cells from younger adults suggesting greater metabolic responses. Conversely, clusters 3 and 4 had increased



expression of the TF ZBED2 in T cells of older adults (Fig. 4e). ZBED2 has been shown to contribute to T cell dysfunction<sup>25</sup>. Of note, only very few cells, all in cluster 4, had evidence of epigenetic or transcriptional hallmarks of differentiated memory cells, such as the *IFNG* gene (Fig. 4e). Cells expressing transcripts for *B3GAT1* and *KLRG1*, typically expressed on CD45RA<sup>+</sup> effector T cells or other effector cytokines were largely not detectable (Extended Data Fig. 7c,d). Overall, these data support that the expansion of cluster 2 or the accelerated chromatin changes in older adults do not reflect recently described, expanded memory cells phenotypically masquerading as naive cells<sup>26</sup>.

### CD25 upregulation is induced by loss of HELIOS with age

As in our studies STAT5 activity in older adults was heightened early in a T cell response, we examined whether aberrant CD25 expression in part already predated activation. Transcripts for *IL2RA* were increased in isolated naive CD4<sup>+</sup> T cells from older adults (Fig. 5a). Flow cytometric studies showed a unimodal distribution of CD25 indicating that expression is a global feature and not limited to a small subset of naive CD4<sup>+</sup> T cells in older adults (Fig. 5b and gating strategy in Extended Data Fig. 8a). Of note, level of CD25 expression was low compared to regulatory T cells. Comparing ATAC-seq of unstimulated naive CD4<sup>+</sup> T cells from young and older adults, we noted putative enhancer regions that were slightly but significantly more open in naive CD4<sup>+</sup> T cells from older adults (Fig. 5c). We transfected the reporter luciferase construct containing the enhancer sequence A<sup>27</sup> into naive CD4<sup>+</sup> T cells from younger and older adults and found 30% higher luciferase activity in older adults (Fig. 5d). We then identified HELIOS as a putative TF binding *IL2RA* enhancers (Extended Data Fig. 8b)<sup>28,29</sup> and examined its occupancy at both enhancers by chromatin immunoprecipitation (ChIP)–qPCR. HELIOS showed a twofold increase in binding in naive CD4<sup>+</sup> T cells from younger compared to older adults (Fig. 5e), indicating it may confer repression of *IL2RA* enhancer activity. We transfected the reporter construct containing the *IL2RA* enhancer A together with forced overexpression of *IKZF2* (encoding HELIOS) and found reduced reporter activity in the presence of HELIOS (Fig. 5f). Moreover, *IKZF2* and *IL2RA* transcripts in naive CD4<sup>+</sup> T cells sorted for CD25 expression inversely correlated (Extended Data Fig. 8c). When comparing transcript and protein levels in naive CD4<sup>+</sup> T cells from younger and older individuals, HELIOS was significantly diminished with age (Fig. 5g,h). Silencing *IKZF2* in resting naive CD4<sup>+</sup> T cells from young adults upregulated CD25 (Fig. 5i), reproducing the patterns seen in older adults. Taken together, *IKZF2* transcripts were low in naive CD4<sup>+</sup> T cells of older adults resulting in CD25 upregulation. As HELIOS is traditionally recognized as a TF maintaining the stability of regulatory T cells<sup>30,31</sup>, the negative relationship between HELIOS and CD25 shown in naive CD4<sup>+</sup> T cells suggests that the subset of CD25<sup>lo</sup>CD4<sup>+</sup>CD45RA<sup>+</sup> T cells increasing with age, are not regulatory T cells.

### HELIOS degradation in CD4<sup>+</sup> T cells induces inflammation

To assess the functional consequences of HELIOS depletion in naive CD4<sup>+</sup> T cells, we used the NSG mouse human chimera model<sup>32</sup>. Human naive CD4<sup>+</sup> T cells were treated with either dimethylsulfoxide (DMSO) or the HELIOS-degrading compound ALV2 (ref. <sup>33</sup>) for 5 d, then activated for 2 d in vitro and finally adoptively transferred together with CD4<sup>+</sup> T cell-depleted, autologous peripheral blood mononuclear cells

(PBMCs) to mice carrying human synovial tissues. ALV2 selectively targets human HELIOS for degradation and we did not find any degradation of murine HELIOS (Fig. 6a). We confirmed upregulation of CD25 and effector cytokine production by ALV2-treated cells after in vitro activation (Fig. 6b and Extended Data Fig. 9a,b). Histological examination showed denser mononuclear infiltrates in synovial tissue implants of mice reconstituted with ALV2-treated T cells (Fig. 6c). Flow cytometry of these tissues confirmed a higher number of tissue-infiltrating, human CD4<sup>+</sup> T cells (Fig. 6d). The increased tissue infiltration was not due to different reconstitution efficiency; the number of human CD4<sup>+</sup> T cells was not different in the spleens of mice having received control or ALV2-treated cells (Extended Data Fig. 9c). Phenotypic characterization revealed higher CD25 and CD38 expression in ALV2-treated cells retrieved from synovial tissues (Fig. 6e). Consistently, we found higher effector T cell transcripts in these tissues (Fig. 6f). Taken together, HELIOS deficiency in naive CD4<sup>+</sup> T cells facilitated differentiation into tissue-invasive T cells and tissue inflammation.

### Rewiring the epigenetic response pattern of older CD4<sup>+</sup> T cells

To determine whether the age-associated signature in activation-induced chromatin remodeling can be prevented, we inhibited STAT5 activity using either IL-2 receptor (IL-2R)-blocking antibodies or a STAT5 inhibitor. Activation-induced epigenetic changes were assessed by ATAC-seq after 48 h. Both IL-2R blocking and STAT5 inhibition of cells from older adults shifted the chromatin accessibility states as defined by PC1 in the direction toward those from younger individuals (Fig. 7a). TF motif enrichment analysis of sites driving PC1 identified STAT and bZIP binding motifs as highly enriched (Fig. 7b). Overall, 25% of differentially opened sites induced by IL-2R blocking or STAT5 inhibition were also differentially open between younger and older adults (indicated by dark red coloring; Fig. 7c and Extended Data Fig. 10a); examples included opening peaks in *TCF7* and *BACH2* and closing peaks in *IRF4* and *BHLHE40* (Fig. 7d and Extended Data Fig. 10b). ChIP–qPCR of naive CD4<sup>+</sup> T cells from older adults after 48-h TCR stimulation confirmed STAT5 binding<sup>34</sup> at the *IRF4* and *BHLHE40* genes (Fig. 7e). Inhibition of IL-2 or STAT5 activity downregulated expression of *IRF4* and *BHLHE40* at the protein level in older adults (Fig. 7f,g and Extended Data Fig. 10c). To determine whether the increased STAT5 activity accounted for the preferential effector over memory CD4<sup>+</sup> T cell generation<sup>13,35</sup>, we determined BLIMP1 (encoded by *PRDM1*) and TCF1 (encoded by *TCF7*) expression after 5 d of TCR activation. pSTAT5 inhibition in cultures with naive CD4<sup>+</sup> T cells from older adults downregulated BLIMP1 and upregulated TCF1 (Fig. 7h), recapitulating the response in young individuals (Fig. 7i), whereas STAT5 inhibition in young did not further bring down BLIMP1 (Extended Data Fig. 10d). Taken together, by dampening IL-2-STAT5 signaling, naive CD4<sup>+</sup> T cells from older adults exhibit a chromatin accessibility state after TCR activation that resembles that in younger adults with increased potential of memory cell formation and reduced inflammatory effector function.

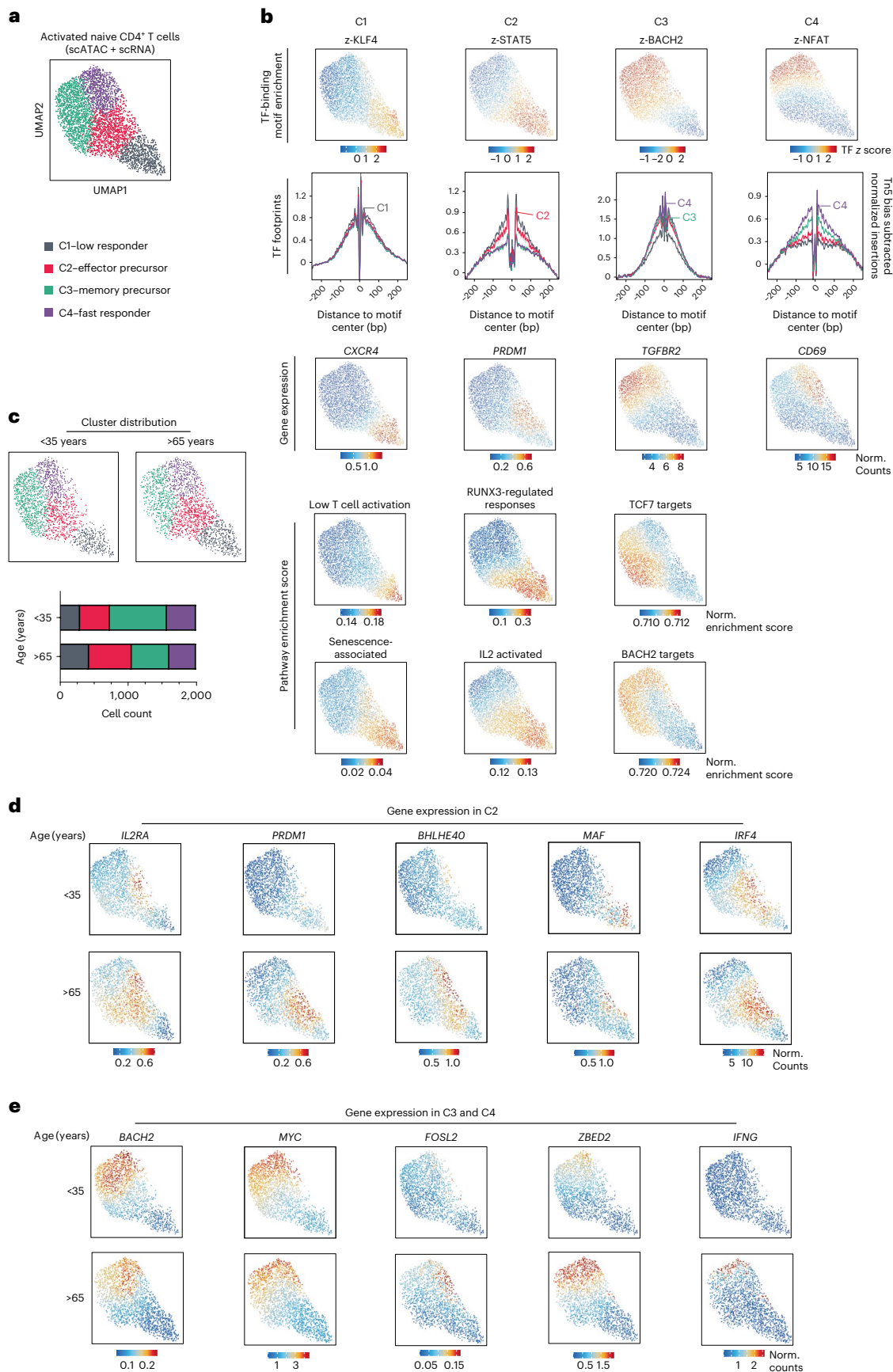
### Discussion

Here, we describe that in spite of attenuated proximal TCR signaling, naive CD4<sup>+</sup> T cells from healthy older adults respond to activation with accelerated remodeling of the epigenome, culminating in increased BATF and BLIMP1 activity. This epigenetic response pattern explains

#### Fig. 4 | Age-associated expansion of naive CD4<sup>+</sup> T cell subsets with increased activation of the STAT5 pathway. a, Naive CD4<sup>+</sup> T cells from two younger and two older individuals were left unstimulated or activated with beads coated with 1 μg ml<sup>-1</sup> anti-CD3 and anti-CD28 for 18 h. Nuclei were subjected to combined scATAC-seq/scRNA-seq. Activated cells were identified in UMAP maps and confirmed by CD69 expression (Extended Data Fig. 7b). UMAP of integrated scATAC-seq and scRNA-seq data are shown with each point representing one cell. Clusters indicated by different colors were generated using Surat graph-clustering approach. b, Representative accessible TF motifs in each

cluster are shown as ChromVAR deviation scores projected on the UMAP map and as footprints using the color code for the different clusters in a (top). Representative gene expression and indicated pathway enrichment scores in each cluster are projected on the UMAP (bottom). c, scMultiomic UMAPs of activated naive CD4<sup>+</sup> T cells from young and older adults are presented separately (top). Frequencies of cells for different clusters are shown as stacked bar graphs (bottom). d, Imputed expression in cluster 2 of genes with differential expression for younger and older adults. e, Genes in cluster 3 and 4 with differential expression for younger and older adults.

cluster are shown as ChromVAR deviation scores projected on the UMAP map and as footprints using the color code for the different clusters in a (top). Representative gene expression and indicated pathway enrichment scores in each cluster are projected on the UMAP (bottom). c, scMultiomic UMAPs of activated naive CD4<sup>+</sup> T cells from young and older adults are presented separately (top). Frequencies of cells for different clusters are shown as stacked bar graphs (bottom). d, Imputed expression in cluster 2 of genes with differential expression for younger and older adults. e, Genes in cluster 3 and 4 with differential expression for younger and older adults.





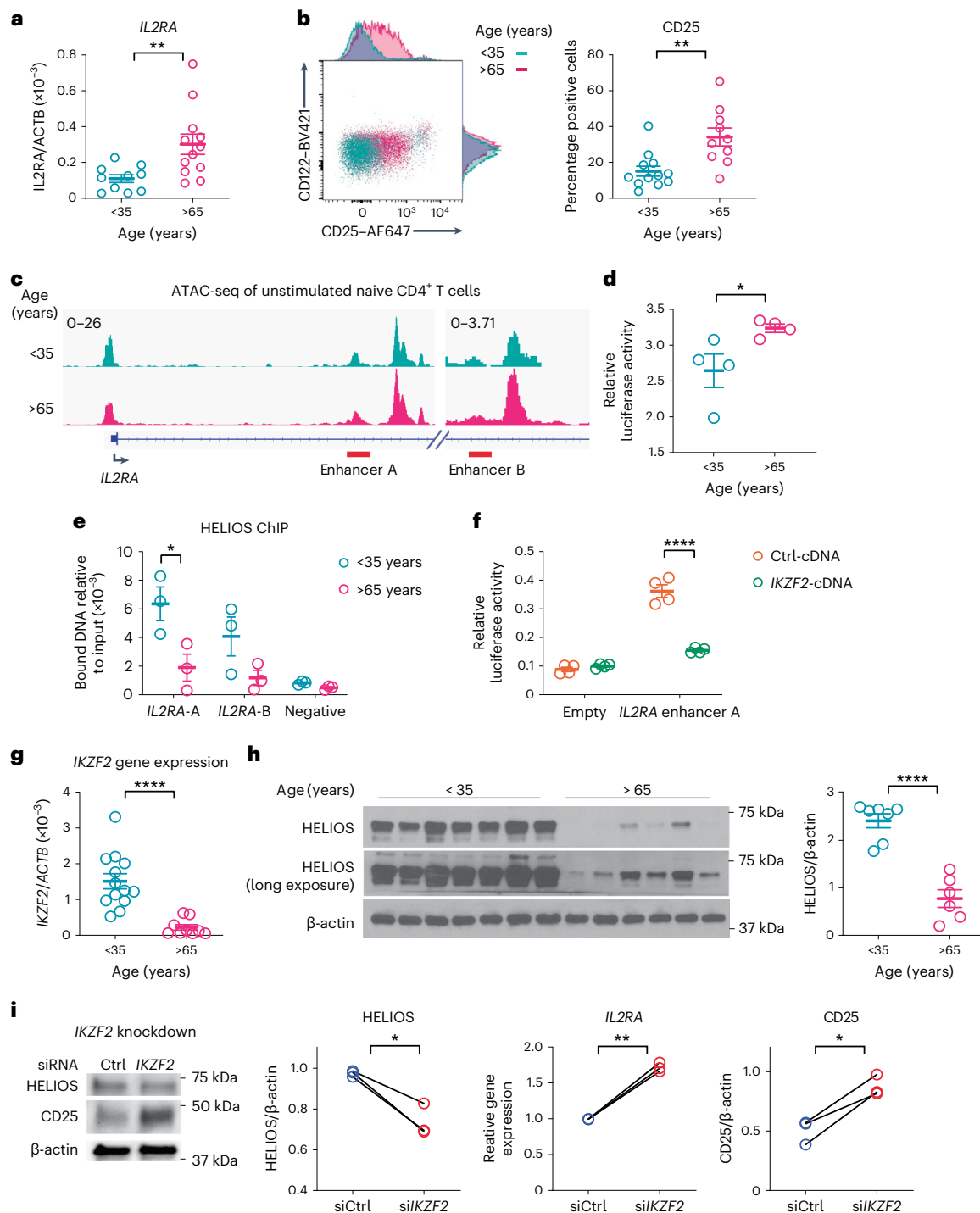


**Fig. 5 | CD25 upregulation is induced by a loss of HELIOS with age.** **a**, *IL2RA* gene expression was quantified in unstimulated naive CD4<sup>+</sup> T cells from 10 younger and 12 older adults. **b**, CD25 was measured by flow cytometry gated on naive CD4<sup>+</sup> T cells (Extended Data Figure 8a) from 12 young and 10 older adults. **c**, Aggregate genome tracks of unstimulated naive CD4<sup>+</sup> T cells from four younger and four older individuals at *IL2RA* enhancer locus (GRCh37, Chr10:6,091,304-6,111,593 and Chr10:6,085,160-6,090,232). **d**, Luciferase activity in unstimulated naive CD4<sup>+</sup> T cells from four younger and four older individuals after transfection of a reporter construct containing *IL2RA* enhancer A. **e**, ChIP-qPCR with HELIOS (encoded by *IKZF2*)-specific antibody of unstimulated naive CD4<sup>+</sup> T cells from three younger and three older adults. **f**, Luciferase activity in unstimulated naive CD4<sup>+</sup> T cells after transfection of reporter construct with or without *IL2RA* enhancer A together with control cDNA or *IKZF2* cDNA.  $n = 4$  biologically

independent samples. **g**, *IKZF2* gene expression in unstimulated naive CD4<sup>+</sup> T cells from 13 younger and 9 older adults. **h**, HELIOS protein expression in unstimulated naive CD4<sup>+</sup> T cells from seven younger and six older adults. Results in **a**, **b**, **d**–**h** are shown as mean  $\pm$  s.e.m. Data were analyzed with two-sided unpaired Student's *t*-test. \* $P < 0.05$  ( $P = 0.048$  for **d**,  $P = 0.041$  for **e**), \*\* $P < 0.01$  ( $P = 0.0087$  for **a**,  $P = 0.0024$  for **b**), \*\*\*\* $P < 0.0001$ . **i**, CD25 expression in unstimulated naive CD4<sup>+</sup> T cells transfected with control or *IKZF2* siRNA. Representative blot of HELIOS and CD25 (left). Summary (right) of data from three experiments for HELIOS protein (left), *IL2RA* transcript (middle) and *IL2RA* protein (right) expression.  $n = 3$  biologically independent samples. Data were analyzed with two-sided paired Student's *t*-test. \* $P < 0.05$  ( $P = 0.02$ ), \*\* $P < 0.01$  ( $P = 0.0025$ ).

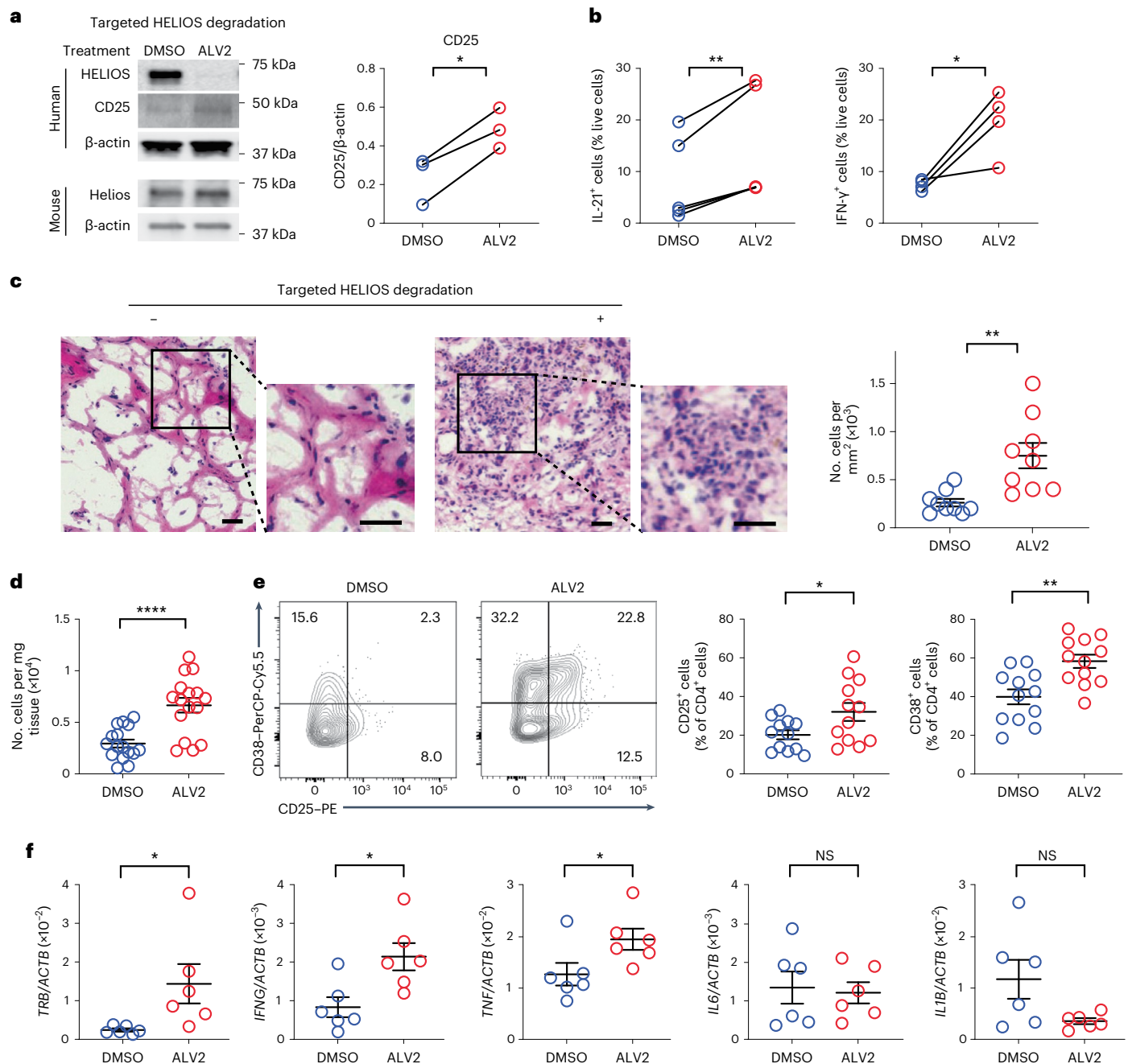


**Fig. 6 | Forced HELIOS degradation in human naive CD4<sup>+</sup> T cells induces tissue inflammation in vivo.** Freshly isolated human naive CD4<sup>+</sup> T cells were cultured with either DMSO as a solvent control or 1 μM ALV2 followed by activation with anti-CD3/anti-CD28. Cultures were continued for in vitro testing or cells were intraperitoneally injected into NSG mice engrafted with human synovial tissues. Seven days after cell injection, tissues were collected for data acquisition. **a**, HELIOS and CD25 expression in unstimulated naive CD4<sup>+</sup> T cells treated with DMSO or 1 μM ALV2 in vitro. Summary of CD25 expression of three experiments.  $n = 3$  biologically independent samples. Data were analyzed with two-sided paired Student's *t*-test. \* $P < 0.05$  ( $P = 0.02$ ). **b**, IL-21 and interferon (IFN)-γ production were measured after 5-d activation in vitro. Summary of three experiments.  $n = 5$  biologically independent samples for IL-21 and  $n = 4$  biologically independent samples for IFN-γ. Data were

analyzed with two-sided paired Student's *t*-test. \*\* $P < 0.01$  ( $p = 0.009$ ), \* $P < 0.05$  ( $P = 0.037$ ). **c**, Representative hematoxylin and eosin (H&E) stains of synovial tissue sections (left) and enumeration of tissue-infiltrating cells using ImageJ (right).  $n = 9$  biologically independent samples. All scale bars indicate 50 μm. **d**, Human CD4<sup>+</sup> T cell number per mg tissue were enumerated by flow cytometry of synovial cells.  $n = 16$  biologically independent samples. **e**, CD25 and CD38 surface expression on tissue-infiltrating CD4<sup>+</sup> T cells were measured with flow cytometry.  $n = 12$  biologically independent samples. **f**, Transcripts of indicated human genes in synovial tissues were quantified and normalized to *ACTB*.  $n = 6$  biologically independent samples. Results in **c–f** are shown as mean ± s.e.m. Data were analyzed with two-sided unpaired Student's *t*-test. \* $P < 0.05$  ( $P = 0.035$  for **e**,  $P = 0.041$ ,  $0.014$ ,  $0.047$  for **f**), \*\* $P < 0.01$  ( $P = 0.0078$  for **c**,  $P = 0.0017$  for **e**), \*\*\*\* $P < 0.001$ . NS, not significant.

why generation of long-lived memory T cells is impaired with age and activated naive T cells are biased to differentiate into effector T cells that are likely to contribute to inflammaging. Single-cell studies integrating ATAC-seq and RNA-seq revealed subsets of T cells with increased

STAT5 activity in older adults early after activation. The increased STAT5 activity accounted for the induction of TF networks that were driving increased chromatin accessibility changes. Addition of a STAT5 inhibitor prevented this epigenetic response pattern and induced TCF1

instead of BLIMP1 expression, a constellation favoring the generation of long-lived memory and follicular helper T ( $T_{FH}$ ) cells.

Based on the attenuation of TCR signaling in T cells from older adults, we expected activation-induced epigenomic changes to be reduced with age and predicted that their induction required increased stimulation strength. In contrast to our expectations, activation-induced remodeling of chromatin accessibility was increased and age-associated differences culminated in the increased expression and activity of BATF. By clustering chromatin accessibility changes according to temporal patterns, we only found one cluster that was more prevalent in T cell responses of younger adults. This cluster involved rapid changes in the first 1–6 h after activation at sites enriched for bZIP family (presumably FRA1 or AP-1), IRF2, NFAT and NUR77 motifs, likely reflecting superior TCR signaling in the younger adults. All other temporal clusters were equally represented in T cell responses from younger and older adults and showed even higher enrichment scores for BATF in older adults in the later clusters.

The TF networks implicated to drive the differential chromatin accessibility changes provide an explanation for earlier functional studies that naive  $CD4^+$  T cells from older adults preferentially develop into effector T cells rather than memory or  $T_{FH}$  cells. Increased pSTAT5 activity accounted for the induction of TF networks characteristic of older T cell responses and was at least in part due to increased expression of CD25. Consistent with previous observations<sup>36</sup>, we found that low levels of CD25 were already found in unstimulated naive  $CD4^+$  T cells of older adults. Heightened IL-2 signaling is known to favor terminal effector differentiation, thereby compromising memory cell formation<sup>37</sup>. In  $CD4^+$  T cells from older adults, this bias toward effector cell differentiation was mechanistically linked to increased expression of miR-21, repressing the expression of several negative regulators of signaling molecules including PTEN, SPRTY and PDCD4 (ref. 13). Besides direct regulation of effector cytokines, STAT5 also induces miR-21 (ref. 38). Moreover, STAT5 inhibits the differentiation of  $T_{FH}$  cells via BLIMP1-dependent repression of BCL6 (ref. 39). In addition to impairing  $T_{FH}$  development, the reduced BCL6 activity derepresses the ecto-ATPase CD39 that is expressed on effector and particularly on exhausted T cells<sup>40,41</sup>. Increased expression of CD39 is a hallmark of T cell responses of older individuals, thereby modifying purinergic signaling<sup>42</sup>. In summary, many observations in older naive  $CD4^+$  T cell responses are explained by increased pSTAT5 signaling.

Integrated scRNA-seq and scATAC-seq analysis showed increased pSTAT5 activity in two clusters of cells that increased with age. Both clusters also shared the enrichment for senescence-like pathways. Cluster 2 cells had heightened CD25 expression and several features of effector cells, including *PRDM1* expression, RUNX3 pathway activity and presence of CD39<sup>+</sup> cells. Notably, neither cluster included fully differentiated effector cells that recently have been reported to be present in the naive compartment<sup>26</sup>. *IFNG* transcript-expressing cells were very few, exclusively assigned to cluster 4 of rapidly responding

cells, and cells expressing *B3GAT1* and *KLRG1* transcripts, hallmarks of end-differentiated effector T cells were largely absent, excluding a major contamination of our naive cell preparation with memory cells.

Beyond these differences related to STAT5 activity, scATAC/RNA-seq also showed an age-associated decrease in *BACH2* and increase in *ZBED2* expression in cluster 3 and 4 cells. *BACH2* has been shown to suppress effector memory-related genes and enforce the transcriptional and epigenetic programs of stem-like  $CD8^+$  T cells, at least in part by controlling access of AP-1 factors to enhancers<sup>23,24</sup>. Thus, *BACH2* deficiency may be an additional mechanism to select against the generation of long-lived memory cells. Notably STAT5 inhibition also restored accessibility to the TFs *BACH2* and *TCF7*. The TF *ZBED2*, also more expressed in older T cells has previously been found enriched in dysfunctional  $CD8^+$  T cells<sup>25</sup>; elevated *ZBED2* expression in older adults may therefore contribute to compromised long-term memory.

We found that naive  $CD4^+$  T cells from older adults were deficient in HELIOS expression and that this deficiency contributed to the increased activation of the pSTAT5–IRF4–BATF TF network. HELIOS acts mainly as a transcriptional repressor in T lymphocytes. It is highly expressed in regulatory T cells; However, regular naive T cells also have a constitutive albeit low expression that is upregulated upon TCR stimulation. Expression of HELIOS in effector memory T cells and especially TEMRAs is high. Studies in HELIOS knockout mice and in patients with loss-of-function mutations support the notion that, in addition to its function in regulatory T cells, HELIOS is a regulator of effector cell differentiation and function<sup>43–45</sup>.

HELIOS is known to interact with chromatin modifiers at the *IL2* locus inducing deacetylation of core histones at the *IL2* promoter<sup>46</sup>. Indeed, T cells from patients with a loss-of-function HELIOS mutation produce increased amount of IL-2 (ref. 43). In our studies, reduced expression of HELIOS in ALV2-treated T cells from younger adults resulted in increased IL-2 production. In addition, we saw an increased inducibility of CD25 due to HELIOS deficiency. The combination of increased IL-2 production and expression of CD25 provides a model that explains the accelerated epigenetic remodeling toward effector functions. Our ability to restore the younger response pattern in older T cells by IL-2R blockade or STAT5 inhibition indicates that this mechanism is a major pathway. Vice versa, HELIOS deficiency is likely to cause defects in T cells other than increased effector differentiation. Clinically, patients with *IKZF2* mutation presented as primary immunodeficiencies<sup>43,45</sup>. It is tempting to speculate that reduced HELIOS expression may have a similar effect in older adults.

Excess STAT5 activity in activated naive  $CD4^+$  T cells can contribute to the inflammatory milieu in older adults through several layers of regulation. STAT5 activity in  $CD4^+$  T cells has been implicated in promoting autoimmune disorders, including experimental autoimmune encephalomyelitis<sup>47</sup> and airway inflammation<sup>48</sup> through upregulation of effector cytokines, such as granulocyte-macrophage colony-stimulating factor and IL-9. Older adults have a bias toward

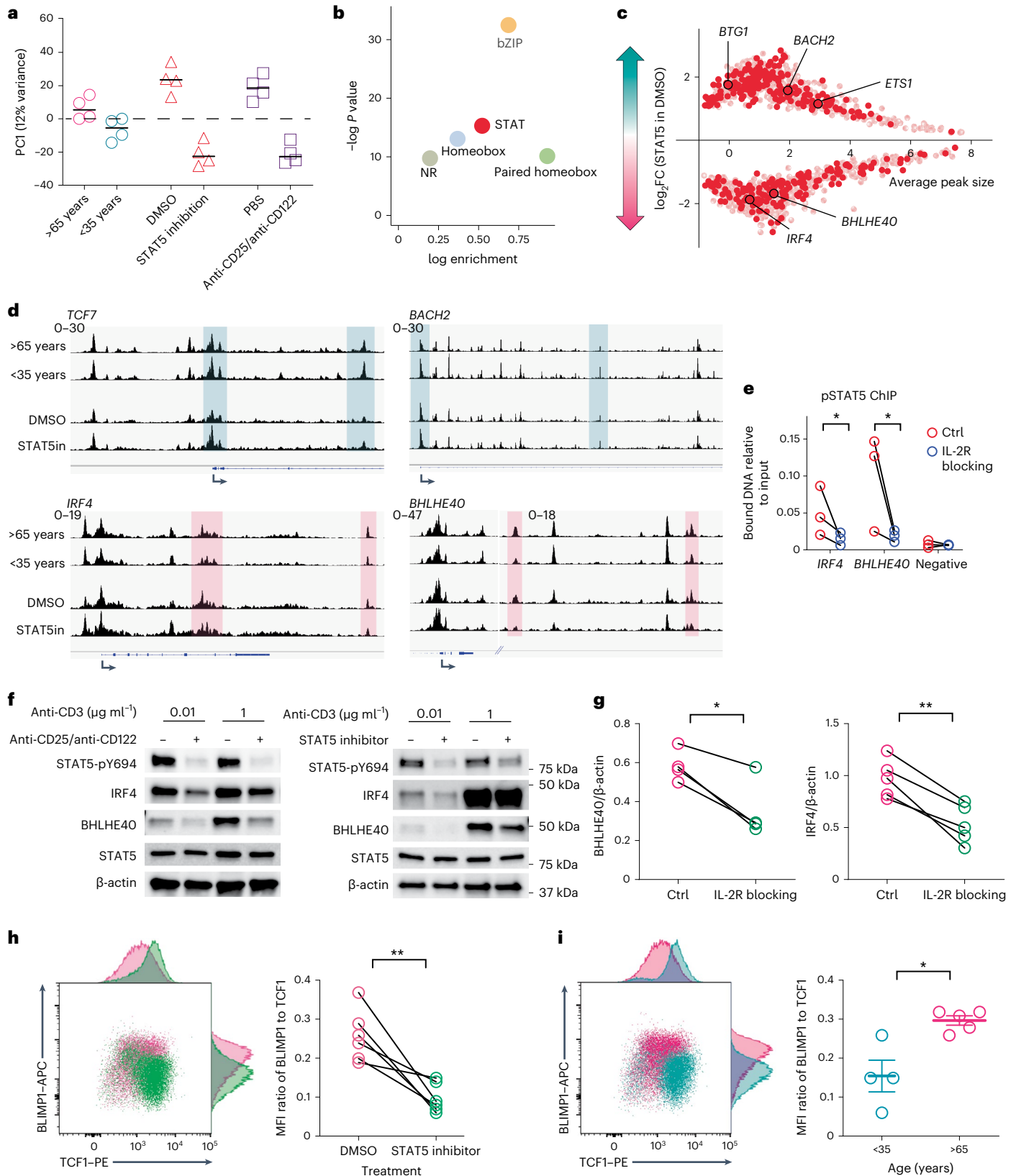
### Fig. 7 | Inhibition of IL-2-STAT5 signaling rewires activated naive $CD4^+$ T cells from older individuals to a younger epigenetic response pattern.

**a**, Naive  $CD4^+$  T cells of older individuals were activated in the presence of either DMSO control, STAT5 inhibitor, PBS control or IL-2R-blocking antibodies for 48 h.  $n = 4$  biologically independent samples. ATAC-seq data from the four treatments together with the 48-h samples from the four young and four older individuals described in Figs. 1a and 2a were subjected to PCA. Results for PC1 are shown. **b**, TF-binding motif enrichment of PC1 loading sites. **c**,  $\text{Log}_2\text{FC}$  of differential peaks between STAT5 inhibition and control are plotted against average peak sizes. Peaks that are also differentially accessible between younger and older individuals are indicated in dark red. Comparisons were conducted by two-sided robust empirical Bayes moderated statistical test. A Benjamini–Hochberg adjusted  $P$  value of 0.05 was used. **d**, Accessibility tracks of representative genes. Magenta indicates peaks that are more open in older adults or with control treatment. Cyan indicates peaks more open in younger adults or with

STAT5 inhibition. **e**, ChIP–qPCR with anti-pSTAT5 antibodies of 48-h activated naive  $CD4^+$  T cells treated as indicated.  $n = 3$  biologically independent samples. **f**, pSTAT5, IRF4 and BHLHE40 were measured in 48-h activated cells for each condition. **g**, Summary of BHLHE40 and IRF4 expression from three experiments of IL-2R blocking.  $n = 4$  biologically independent samples for BHLHE40 and  $n = 5$  for IRF4. **h**, Naive  $CD4^+$  T cells from older adults were activated with  $1 \mu\text{g ml}^{-1}$  anti-CD3-coated beads for 5 d with DMSO control or a STAT5 inhibitor. BLIMP1 and TCF1 expression were measured by flow cytometry in six experiments. The MFI ratio of BLIMP1 to TCF1 was plotted.  $n = 6$  biologically independent samples. **i**, Naive  $CD4^+$  T cells from younger and older adults were activated for 5 d. BLIMP1 and TCF1 protein expression was assayed as in **h**. Results are shown as mean  $\pm$  s.e.m.  $n = 9$  biologically independent samples. Data were analyzed with two-sided paired Student's  $t$ -test (**e**, **g**, **h**) and two-sided unpaired Student's  $t$ -test (**i**). \* $P < 0.05$  ( $P = 0.01$  for IRF4 and 0.02 for BHLHE40 in **e**,  $P = 0.01$  for **g**,  $P = 0.02$  for **i**), \*\* $P < 0.01$  ( $P = 0.0028$  for **g**,  $P = 0.0071$  for **h**).

T<sub>H</sub>9 cell generation through upregulated IRF4 and BATF<sup>49</sup>. Increased effector T cell differentiation driven by IL-2 signaling may therefore be an important regulator of inflammaging as well as the excessive inflammation seen in some older adults in the course of an antiviral

response. Identification of IL-2 signaling as an upstream regulator of age-related epigenetic differences in T cell responses provides a new target to attenuate inflammatory responses and improve memory cell generation.



## Online content

Any methods, additional references, Nature Portfolio reporting summaries, source data, extended data, supplementary information, acknowledgements, peer review information; details of author contributions and competing interests; and statements of data and code availability are available at <https://doi.org/10.1038/s41590-022-01369-x>.

## References

- O'Driscoll, M. et al. Age-specific mortality and immunity patterns of SARS-CoV-2. *Nature* **590**, 140–145 (2021).
- Rydzynski Moderbacher, C. et al. Antigen-specific adaptive immunity to SARS-CoV-2 in acute COVID-19 and associations with age and disease severity. *Cell* **183**, 996–1012 (2020).
- Gustafson, C. E., Kim, C., Weyand, C. M. & Goronzy, J. J. Influence of immune aging on vaccine responses. *J. Allergy Clin. Immunol.* **145**, 1309–1321 (2020).
- Weng, N. P. Aging of the immune system: how much can the adaptive immune system adapt? *Immunity* **24**, 495–499 (2006).
- Furman, D. et al. Chronic inflammation in the etiology of disease across the life span. *Nat. Med.* **25**, 1822–1832 (2019).
- Goronzy, J. J. & Weyand, C. M. Mechanisms underlying T cell ageing. *Nat. Rev. Immunol.* **19**, 573–583 (2019).
- Mittelbrunn, M. & Kroemer, G. Hallmarks of T cell aging. *Nat. Immunol.* **22**, 687–698 (2021).
- Whiting, C. C. et al. Large-scale and comprehensive immune profiling and functional analysis of normal human aging. *PLoS ONE* **10**, e0133627 (2015).
- Qi, Q. et al. Diversity and clonal selection in the human T-cell repertoire. *Proc. Natl Acad. Sci. USA* **111**, 13139–13144 (2014).
- Fülöp, T. et al. Age-related impairment of p56lck and ZAP-70 activities in human T lymphocytes activated through the TcR/CD3 complex. *Exp. Gerontol.* **34**, 197–216 (1999).
- Li, G. et al. Decline in miR-181a expression with age impairs T cell receptor sensitivity by increasing DUSP6 activity. *Nat. Med.* **18**, 1518–1524 (2012).
- Pereira, B. I. et al. Sestrins induce natural killer function in senescent-like CD8<sup>+</sup> T cells. *Nat. Immunol.* **21**, 684–694 (2020).
- Kim, C. et al. Activation of miR-21-regulated pathways in immune aging selects against signatures characteristic of memory T cells. *Cell Rep.* **25**, 2148–2162 (2018).
- Goronzy, J. J. & Weyand, C. M. Successful and maladaptive T cell aging. *Immunity* **46**, 364–378 (2017).
- Elyahu, Y. et al. Aging promotes reorganization of the CD4 T cell landscape toward extreme regulatory and effector phenotypes. *Sci. Adv.* **5**, eaaw8330 (2019).
- Almanzar, N. et al. A single-cell transcriptomic atlas characterizes ageing tissues in the mouse. *Nature* **583**, 590–595 (2020).
- Mogilenko, D. A. et al. Comprehensive profiling of an aging immune system reveals clonal GZMK<sup>+</sup>CD8<sup>+</sup> T cells as conserved hallmark of inflammaging. *Immunity* **54**, 99–115 (2021).
- den Braber, I. et al. Maintenance of peripheral naive T cells is sustained by thymus output in mice but not humans. *Immunity* **36**, 288–297 (2012).
- Zhang, H., Weyand, C. M. & Goronzy, J. J. Hallmarks of the aging T-cell system. *FEBS J.* **288**, 7123–7142 (2021).
- Kaech, S. M., Hemby, S., Kersh, E. & Ahmed, R. Molecular and functional profiling of memory CD8 T cell differentiation. *Cell* **111**, 837–851 (2002).
- Kurachi, M. et al. The transcription factor BATF operates as an essential differentiation checkpoint in early effector CD8<sup>+</sup> T cells. *Nat. Immunol.* **15**, 373–383 (2014).
- Davenport, M. P., Smith, N. L. & Rudd, B. D. Building a T cell compartment: how immune cell development shapes function. *Nat. Rev. Immunol.* **20**, 499–506 (2020).
- Roychoudhuri, R. et al. BACH2 regulates CD8<sup>+</sup> T cell differentiation by controlling access of AP-1 factors to enhancers. *Nat. Immunol.* **17**, 851–860 (2016).
- Yao, C. et al. BACH2 enforces the transcriptional and epigenetic programs of stem-like CD8<sup>+</sup> T cells. *Nat. Immunol.* **22**, 370–380 (2021).
- Li, H. et al. Dysfunctional CD8 T cells form a proliferative, dynamically regulated compartment within human melanoma. *Cell* **176**, 775–789 (2019).
- Pulko, V. et al. Human memory T cells with a naive phenotype accumulate with aging and respond to persistent viruses. *Nat. Immunol.* **17**, 966–975 (2016).
- Simeonov, D. R. et al. Discovery of stimulation-responsive immune enhancers with CRISPR activation. *Nature* **549**, 111–115 (2017).
- Kent, W. J. et al. The human genome browser at UCSC. *Genome Res.* **12**, 996–1006 (2002).
- Rosenbloom, K. R. et al. ENCODE data in the UCSC genome browser: year 5 update. *Nucleic Acids Res.* **41**, D56–D63 (2013).
- Kim, H. J. et al. Stable inhibitory activity of regulatory T cells requires the transcription factor Helios. *Science* **350**, 334–339 (2015).
- Thornton, A. M. et al. Expression of Helios, an Ikaros transcription factor family member, differentiates thymic-derived from peripherally induced Foxp3<sup>+</sup> regulatory cells. *J. Immunol.* **184**, 3433–3441 (2010).
- Yang, Z. et al. Restoring oxidant signaling suppresses proarthritogenic T cell effector functions in rheumatoid arthritis. *Sci. Transl. Med.* **8**, 331ra338 (2016).
- Wang, E. S. et al. Acute pharmacological degradation of Helios destabilizes regulatory T cells. *Nat. Chem. Biol.* **17**, 711–717 (2021).
- Liao, W., Lin, J.-X., Wang, L., Li, P. & Leonard, W. J. Modulation of cytokine receptors by IL-2 broadly regulates differentiation into helper T cell lineages. *Nat. Immunol.* **12**, 551–559 (2011).
- Jin, J. et al. Activation of mTORC1 at late endosomes misdirects T cell fate decision in older individuals. *Sci. Immunol.* **6**, 791–791 (2021).
- Pekalski, M. L. et al. Postthymic expansion in human CD4 naive T cells defined by expression of functional high-affinity IL-2 receptors. *J. Immunol.* **190**, 2554–2566 (2013).
- Kalia, V. et al. Prolonged interleukin-2R $\alpha$  expression on virus-specific CD8<sup>+</sup> T cells favors terminal-effector differentiation in vivo. *Immunity* **32**, 91–103 (2010).
- Lindahl, L. M. et al. STAT5 induces miR-21 expression in cutaneous T cell lymphoma. *Oncotarget* **7**, 45730–45744 (2016).
- Johnston, R. J., Choi, Y. S., Diamond, J. A., Yang, J. A. & Crotty, S. STAT5 is a potent negative regulator of T<sub>FH</sub> cell differentiation. *J. Exp. Med.* **209**, 243–250 (2012).
- Canale, F. P. et al. CD39 expression defines cell exhaustion in tumor-infiltrating CD8<sup>+</sup> T cells. *Cancer Res.* **78**, 115–128 (2018).
- Cao, W. et al. Ecto-NTPDase CD39 is a negative checkpoint that inhibits follicular helper cell generation. *J. Clin. Invest.* **130**, 3422–3436 (2020).
- Fang, F. et al. Expression of CD39 on activated T cells impairs their survival in older individuals. *Cell Rep.* **14**, 1218–1231 (2016).
- Hetemäki, I. et al. Loss-of-function mutation in IKZF2 leads to immunodeficiency with dysregulated germinal center reactions and reduction of MAIT cells. *Sci. Immunol.* **6**, 3454 (2021).
- Serre, K. et al. Helios is associated with CD4 T cells differentiating to T helper 2 and follicular helper T cells in vivo independently of Foxp3 expression. *PLoS ONE* **6**, e20731 (2011).
- Shahin, T. et al. Germline biallelic mutation affecting the transcription factor Helios causes pleiotropic defects of immunity. *Sci. Immunol.* **6**, 3981 (2021).

46. Baine, I., Basu, S., Ames, R., Sellers, R. S. & Macian, F. Helios induces epigenetic silencing of IL2 gene expression in regulatory T cells. *J. Immunol.* **190**, 1008 (2013).
47. Sheng, W. et al. STAT5 programs a distinct subset of GM-CSF-producing T helper cells that is essential for autoimmune neuroinflammation. *Cell Res.* **24**, 1387–1402 (2014).
48. Fu, Y. et al. STAT5 promotes accessibility and is required for BATF-mediated plasticity at the Il9 locus. *Nat. Commun.* **11**, 1–16 (2020).
49. Hu, B. et al. Transcription factor networks in aged naive CD4 T cells bias lineage differentiation. *Aging Cell* **18**, e12957 (2019).

**Publisher's note** Springer Nature remains neutral with regard to jurisdictional claims in published maps and institutional affiliations.

Springer Nature or its licensor (e.g. a society or other partner) holds exclusive rights to this article under a publishing agreement with the author(s) or other rightsholder(s); author self-archiving of the accepted manuscript version of this article is solely governed by the terms of such publishing agreement and applicable law.

© The Author(s), under exclusive licence to Springer Nature America, Inc. 2022

## Methods

### Study design

For sequencing studies, 16 individuals were recruited who did not have an acute or active chronic disease or a history of cancer or autoimmune diseases. Chronic diseases such as hypertension were permitted if controlled by medication. The studies were approved by the Stanford University and Mayo Clinic Institutional Review Boards and all participants gave informed written consent. Basic demographic information is listed in Supplementary Table 1. Naive CD4<sup>+</sup> T cells from participants 1–8 were stimulated with polystyrene beads coated with 0, 0.01 and 1  $\mu\text{g ml}^{-1}$  anti-CD3 (BioLegend, no. 317320) and 1  $\mu\text{g ml}^{-1}$  anti-CD28 (Miltenyi Biotec, no. 130-093-386) for 1.5, 6, 24 and 48 h. All 96 samples were collected for ATAC-seq. RNA-seq was performed on the eight unstimulated samples and the 64 anti-CD3-stimulated samples. Naive CD4<sup>+</sup> T cells from individuals 9–12 were stimulated with polystyrene beads (1  $\mu\text{g ml}^{-1}$  anti-CD3 and anti-CD28) for 18 h and collected for scMultiome sequencing. Naive CD4<sup>+</sup> T cells from individuals 13–16 were stimulated with polystyrene beads (1  $\mu\text{g ml}^{-1}$  anti-CD3) for 48 h in presence of either PBS, 5  $\mu\text{g ml}^{-1}$  anti-CD25 and anti-CD122, DMSO solvent control or 50  $\mu\text{M}$  STAT5 inhibitor (Cayman Chemical, no. 15784) in DMSO. For experiments not involving genome-wide sequencing, samples were obtained from leukocyte reduction system (LRS) cones or buffy coats from de-identified donors ( $n = 123$ , age 21–35 years or over 65 years) through the Stanford Blood Bank and Mayo Clinic Blood Bank.

### Naive CD4<sup>+</sup> T cell isolation and activation

PBMCs were Ficoll-isolated from buffy coats or LRS cones. Naive CD4<sup>+</sup> T cells were isolated by negative selection with EasySep Human naive CD4<sup>+</sup> T Cell Isolation kit (Stemcell, no. 19555). Purity of naive CD4<sup>+</sup> T cells was examined with surface staining of CD4, CD45RA and CD62L (Supplementary Table 2). For time course studies, cells were rested overnight in RPMI medium (Sigma, no. R8758) and then stimulated with polystyrene beads labeled with anti-CD3 at 0, 0.01 or 1  $\mu\text{g ml}^{-1}$  and anti-CD28 at 1  $\mu\text{g ml}^{-1}$  in a 96-well round-bottom plate. Each well contained 200,000 cells and an equal number of beads in 200  $\mu\text{l}$  RPMI medium. To synchronize TCR stimulation, plates were centrifuged for 3 min at 500  $g$ . At indicated times, cells were washed with PBS and subjected to ATAC-seq, RNA-seq or scMultiome experiments.

### Polystyrene beads labeling

Streptavidin-coated polystyrene beads (Bangs Laboratories, no. CP01006) were washed with 1 $\times$  PBS/1%FBS and mixed with biotinylated anti-CD28 (Miltenyi Biotec, no. 130-093-386) at 1  $\mu\text{g ml}^{-1}$  and biotinylated anti-CD3 (BioLegend, no. 317320) at 0, 0.01 or 1  $\mu\text{g ml}^{-1}$  in 10 $\times$  PBS/1%FBS for 20 min. The amount of anti-CD28 was optimized to maximize binding of cells to beads irrespective of anti-CD3 concentration (Extended Data Fig. 1). Labeled beads were washed twice with 1 $\times$  PBS/1%FBS and resuspended in RPMI medium.

### IKZF2 knockdown in unstimulated naive CD4<sup>+</sup> T cells

Cells were transfected with either ON-TARGETplus short interfering RNA (siRNA) negative control (Horizon, no. D-001810-10-20) or siRNA targeting *IKZF2* (Horizon, no. L-006946-00-0005) using the Amaxa Nucleofector system and P3 Primary Cell 4D-Nucleofector X kit (Lonza, no. V4XP-3024). At 2 h after transfection, cells were collected and resuspended in prewarmed medium and cultured for 2 d before collection and analysis.

### Flow cytometry

Surface protein labeling was performed by mixing cells with antibodies in 1 $\times$  PBS/1%FBS. For phosphorylated protein staining, cells were fixed (BD, no. 554655), permeabilized (BD, no. 558050) and stained with antibodies. For TF staining, cells were fixed (BD, no. 554655), permeabilized (eBioscience, no. 00-8333-56) and stained with antibodies

(Supplementary Table 2). Stained samples were acquired with BD LSR Fortessa FACSDiva (v.8.0) and analyzed with FlowJo v.9.

### ATAC-seq

A total of 50,000 cells were collected for standard transposition reactions<sup>50</sup> and sequenced with NovaSeq 6000 by the Genome Sequencing Service Center at Stanford University. The ATAC-seq reads were preprocessed to remove adaptors followed by filtering for read quality cutoff of 20. The reads were further filtered to select only autosomal reads for further analysis. The reads were mapped to the hg19 genome using bowtie. Peak calling was performed using macs followed by generating a consensus peak set present in at least three samples with more than 50% site overlap. Reads were assigned to the consensus peaks using feature counts and used for downstream analysis. Samples were separated into groups based on the anti-CD3 concentration, time point and age. PCA and UMAP were performed on counts normalized using variance stabilizing transformation (vst) followed by removing batch effect for donors (except for aging comparison) from DESeq2. Deviations in TF motif accessibility patterns were estimated on all consensus peaks using ChromVAR<sup>51</sup>. Differential accessibility was assessed on data quantile normalized using voomWithQualityWeights from limma with addition of offsets from conditional quantile normalization (CQN)<sup>52</sup> to account for GC content bias. We used duplicateCorrelation to control for donor effects followed by fitting a robust linear regression model with sample correlation blocking for donors. The differences between sample groups were estimated by fitting contrasts to the model followed by a robust empirical Bayes moderation and by the Benjamini–Hochberg procedure to control for false discovery rate. We used contrasts to identify aggregate differences across all time points or age groups while controlling for baseline changes at each time point. The identified differential sites were further median normalized across sample groups and used to identify clusters using  $k$ -means clustering. Gap statistics was used to determine number of clusters in the data with a cutoff at ten clusters. The differential sites were annotated with associated genes using GREAT and used for downstream analysis and comparisons with RNA-seq<sup>53</sup>. Gene ontology analysis was conducted using ChIPseeker<sup>54</sup>.

### RNA-seq

A total of 150,000 cells were collected for RNA extraction. RNA libraries were generated with universal plus mRNA-seq kit (Nugene, no. 0520-A01) and sequenced with NovaSeq 6000 by Novogene Corporation. RNA-seq reads were preprocessed using the nf-core RNA-seq pipeline v.1.4.2 to determine reads mapped to genes in GRCh37 genome. The preprocessing for downstream analysis was kept consistent with ATAC-seq as follows. For PCA and UMAP, the RNA-seq read counts were normalized by 'vst' followed by removing batch effect for donors (except for aging comparison) using DESeq2. To identify differential transcripts, we used CQN offsets along with quantile normalized data from voomWithQualityWeights from limma. We also used duplicateCorrelation to control for donor effects followed by fitting a robust linear regression, blocking for donor and accounting for sample correlation. The differentially expressed genes between groups were estimated by fitting contrasts to the model followed by a robust empirical Bayes moderation and by the Benjamini–Hochberg procedure to control for false discovery rate. The contrasts were setup to identify aggregate differences in transcripts controlling for only baseline changes. The differential genes were further median normalized and used for  $k$ -means clustering. Gap statistics was used to determine the number of clusters in the data with a cutoff of ten clusters.

### TCseq

Fuzzy  $c$ -means cluster analysis of the ATAC-seq dataset was conducted using the TCseq package in R. First, the set of sites for analysis was defined as the union of peak locations detected by MACS2 from all time points. This set was then filtered for genomic regions that showed

a significant change in read counts over time. Differential read count analysis used a negative binomial generalized linear model implemented by edgeR. Finally, the time course of normalized read counts at each genomic interval was clustered using soft clustering ('fuzzy c-means'). To reduce the bias introduced by differences in absolute values, data were standardized using a z score transformation before clustering. We tested a range of starting seed clusters (2–10) to find the optimum minimal number of clusters for capturing distinctive temporal patterns in the data.

### Single-cell multiome (scATAC-seq and scRNA-seq)

Naive CD4<sup>+</sup> T cells were left unstimulated or stimulated for 18 h with 1 µg ml<sup>-1</sup> anti-CD3-coated beads. A total of 40,000 cells were collected and subjected to low-input nuclei isolation. A total of 10,000 nuclei from individuals 9 and 10 and 10,000 nuclei from individuals 11 and 12 were pooled for library generation (Supplementary Table 1). scATAC and gene expression libraries from each pool were generated at the Stanford Genomics Core following the Chromium Next GEM Single Cell Multiome ATAC + Gene Expression User Guide and sequenced with NovaSeq 6000 by Novogene Corp. The multiome data for scRNA-seq and scATAC-seq were processed using CellRanger ARC followed by ArchR<sup>55</sup>. Pathway enrichment scores were calculated by Ucell package in R using the following datasets from MSigDB<sup>56,57</sup>: low T cell activation (GSE22886)<sup>58</sup>, RUNX3-regulated genes (Reactome R-HSA-8949275), TCF7 targets<sup>59</sup>, senescence-associated genes (Reactome R-HSA-2559584), IL-2-activated genes (GSE8685)<sup>60</sup> and BACH2 targets<sup>59</sup>.

### ChIP-qPCR

ChIP assays were performed using the ChIP-IT kit (53040, Active Motif) according to the manufacturer's instruction. Briefly, 5 × 10<sup>6</sup> cells were fixed with fixation buffer (containing 1% formaldehyde), washed and sonicated on ice with a sonicator (Active Motif) to obtain 100–1,000-bp DNA fragments. Fragmented DNA was immunoprecipitated with pSTAT5 and HELIOS-specific antibodies (Supplementary Table 2). Immunoprecipitated DNA were purified and subjected to qPCR using the following primers:

IRF4 (5'-AGTTGCAGTTGACCTACGG-3', 5'-TTCGATCGTCTGA GATGCTG-3');

BHLHE40 (5'-GCCTGTTGACACAACGTAC-3', 5'-GATCAGTTT CTGCTGACGC-3');

IL2RA-A (5'-TGATCCGTATCTTGCCCTCC-3', 5'-GAAACTCCAG GGCAACAAAG-3');

IL2RA-B (5'-CCACCCACTCTTTGCTGGAT-3', 5'-TCAATGGGTAA CAGCACCAGT-3');

Negative control (5'-AACCTGCAAACATGGTTATTT-3', 5'-AA TTTGCCCAAACAGCAAGT-3').

### qPCR

RNA was extracted with an RNeasy Micro kit (QIAGEN, no. 74004) and reverse-transcribed with a High-Capacity cDNA Reverse Transcription kit (Thermo Fisher, no. 4368814). qPCR was performed with PowerUp SYBR Green Master Mix (Thermo Fisher, no. A25776) and the primers listed below and analyzed with QuantStudio Design and Analysis v.2.5.

IKZF2 (5'-GCTCCTCGTGAAGATGGAG-3', 5'-TGCCTAACGTG TGTGTTGTC-3');

IL2RA (5'-ATTTCTGTTGGGGCAGATG-3', 5'-TCTCTTACC TGAAACTGACTG-3');

TRB (5'-CCTTCAACAACAGCATTATCCAG-3', 5'-CGAGGGG CACAGGCTGTCTT-3');

IFNG (5'-ACTAGGCAGCCAACCTAAGCAAGA-3', 5'-CATCAGGGT CACCTGACACATTCA-3');

TNF (5'-CGCATCGCCGCTCCTACCA-3', 5'-AGGGCAATGATCC CAAAGTA-3');

ACTB (5'-GATCATTGCTCCTCCTGAGC-3', 5'-CGTCATACTCCTG CTTGCTG-3').

### Luciferase reporter assay

HEK-293T cells were cotransfected with empty pGL4.23 (Promega, no. E8411) or pGL4.23-IL2RA CaRE4 plasmid<sup>27</sup> and Renilla luciferase reporter plasmid, a HELIOS-expressing plasmid (Sino Biological, no. HG19573-UT) or a control vector (Sino Biological, no. CV011). After 48 h, luciferase activities were measured with the Dual-Luciferase Reporter Assay System (Promega, no. E1910) according to the manufacturer's instructions. For measuring IL2RA enhancer activity in human T cells, pGL4.23-IL2RA CaRE4 and Renilla plasmid were cotransfected into unstimulated naive CD4<sup>+</sup> T cells using the Amaxa Nucleofector system and P3 Primary Cell 4D-Nucleofector X kit (Lonza, no. V4XP-3024). Cells were cultured with IL-7 for 3 d and subjected to luciferase activity measurement.

### Immunoblot

Cells were lysed with RIPA buffer (Thermo Fisher, no. 89900) supplemented with protease and phosphatase inhibitors (Thermo Fisher, no. 78441). Protein lysates were loaded on 4–15% precast TGX gels (BioRad, no. 4561086) and transferred to nitrocellulose membranes (BioRad, no. 1704270). Membranes were blocked with 5% milk in PBST buffer and incubated at 4 °C overnight with primary antibodies (Supplementary Table 2). After washing twice with PBST buffer, membranes were incubated with secondary antibodies (Cell Signaling, no. 7074) for 1 h and washed twice. Chemiluminescent signals were developed with SuperSignal West Femto Maximum Sensitivity Substrate (Thermo Fisher, no. 34095).

### Human-synovium-SCID mouse chimeras

Human-synovium-SCID mouse chimeras were generated as previously reported<sup>32</sup>. Briefly, NSG mice were purchased from the Jackson Laboratory. Both male and female mice were used at age 10–12 weeks. Mice were subcutaneously implanted with pieces of human synovial tissues. In parallel, purified human naive CD4<sup>+</sup> T cells were cultured with DMSO as solvent control or 1 µM ALV2 (ref. 33) for 5 d and then activated for 2 d by 5 µg ml<sup>-1</sup> plate-immobilized anti-CD3 and 1 µg ml<sup>-1</sup> anti-CD28. Chimeric mice engrafted with synovial tissues from the same donor were randomly assigned to control or ALV2-treated cells. Seven days after engraftment, mice were intraperitoneally injected with 4 × 10<sup>6</sup> of the treated CD4<sup>+</sup> T cells combined with 10 × 10<sup>6</sup> autologous, untreated PBMCs depleted of CD4<sup>+</sup> T cells. Human synovial tissues and mouse spleens were collected 1 week after adoptive transfer. Synovial tissues were digested with 1.5 mg ml<sup>-1</sup> collagenase I for 30 min to retrieve cells for flow cytometry staining or OCT-embedded for H&E stains and RNA extraction. Mouse spleens were collected and stained for human CD4<sup>+</sup> T cells. All protocols were approved by the Mayo Clinic Animal Care and Use Committee.

### Statistical analysis

Statistical analysis was performed using Prism 7.0 software. Two-tailed paired or unpaired Student's *t*-tests were used for comparing two groups. Sample sizes to identify differences between younger and older adults were chosen to ensure 80% power with a level of significance of 5% for a difference of their means of 1.5 s.d. ( $n \geq 10$ ). Data distribution was not formally tested but was assumed to be normal. To assess the effect of in vitro intervention (for example, gene silencing and pharmacological inhibition), we used paired testing with sample sizes of three to five. Sample sizes for the mouse chimera studies<sup>61,62</sup> and the ATAC-seq and RNA-seq studies<sup>63</sup> were similar to those reported in previous publications.  $P < 0.05$  was considered statistically significant. No data were excluded from the analyses. The experiments were not randomized. The investigators were not blinded to allocation during the experiments and outcome assessment. Statistical details and significance levels can be found in figure legends.

### Reporting summary

Further information on research design is available in the Nature Portfolio Reporting Summary linked to this article.



## Data availability

Raw sequencing data have been deposited in SRA with the BioProject accession no. [PRJNA757466](https://www.ncbi.nlm.nih.gov/bioproject/PRJNA757466). Raw experimental data will be provided by the corresponding author upon request. Source data are provided with this paper.

## References

50. Buenrostro, J. D., Wu, B., Chang, H. Y. & Greenleaf, W. J. ATAC-seq: a method for assaying chromatin accessibility genome-wide. *Curr. Protoc. Mol. Biol.* **109**, 21.29.21–21.29.29 (2015).
51. Schep, A. N., Wu, B., Buenrostro, J. D. & Greenleaf, W. J. chromVAR: inferring transcription-factor-associated accessibility from single-cell epigenomic data. *Nat. Methods* **14**, 975–978 (2017).
52. Hansen, K. D., Irizarry, R. A. & Wu, Z. Removing technical variability in RNA-seq data using conditional quantile normalization. *Biostatistics* **13**, 204–216 (2012).
53. McLean, C. Y. et al. GREAT improves functional interpretation of cis-regulatory regions. *Nat. Biotechnol.* **28**, 495–501 (2010).
54. Yu, G., Wang, L.-G. & He, Q.-Y. ChIPseeker: an R/Bioconductor package for ChIP peak annotation, comparison and visualization. *Bioinformatics* **31**, 2382–2383 (2015).
55. Granja, J. M. et al. ArchR is a scalable software package for integrative single-cell chromatin accessibility analysis. *Nat. Genet.* **53**, 403–411 (2021).
56. Liberzon, A. et al. Molecular signatures database (MSigDB) 3.0. *Bioinformatics* **27**, 1739–1740 (2011).
57. Subramanian, A. et al. Gene set enrichment analysis: A knowledge-based approach for interpreting genome-wide expression profiles. *Proc. Natl Acad. Sci. USA* **102**, 15545–15550 (2005).
58. Abbas, A. R. et al. Immune response in silico (IRIS): immune-specific genes identified from a compendium of microarray expression data. *Genes Immun.* **6**, 319–331 (2005).
59. Kolmykov, S. et al. GTRD: an integrated view of transcription regulation. *Nucleic Acids Res.* **49**, D104–D111 (2021).
60. Marzec, M. et al. Differential effects of interleukin-2 and interleukin-15 versus interleukin-21 on CD4<sup>+</sup> cutaneous T-cell lymphoma cells. *Cancer Res.* **68**, 1083–1091 (2008).
61. Wen, Z. et al. N-myristoyltransferase deficiency impairs activation of kinase AMPK and promotes synovial tissue inflammation. *Nat. Immunol.* **20**, 313–325 (2019).
62. Wu, B. et al. Mitochondrial aspartate regulates TNF biogenesis and autoimmune tissue inflammation. *Nat. Immunol.* **22**, 1551–1562 (2021).
63. Moskowitz, D. M. et al. Epigenomics of human CD8 T cell differentiation and aging. *Sci. Immunol.* **2**, eaag0192 (2017).

## Acknowledgements

This work was supported by the National Institutes of Health (R01 ARO42527, R01 HL117913, R01 AI108906, R01 HL142068 and P01 HL129941 to C.M.W. and R01 AI108891, R01 AG045779, U19 AI057266 and R01 AI129191 to J.J.G.). The content is solely the responsibility of the authors and does not necessarily represent the official views of the National Institutes of Health. We thank E. Fischer from Harvard Medical School for providing the ALV2 compound, P. Li from the National Institutes of Health for providing processed ChIP-seq data files of human CD4<sup>+</sup> T cells, C. Gustafson and F. Müller for suggestions on single-cell data analysis, X. Wang and F. Cao for suggestions on ATAC-seq time course analysis and the Stanford Genome Sequencing Service Center and Novogen for providing sequencing services.

## Author contributions

H.Z., R.R.J., W.J.G., C.M.W. and J.J.G. designed the research and interpreted data. H.Z., W.C., T.Z., J.J., S.O., J.M. and Z.H. performed experimental work. R.R.J. and I.N.G. analyzed high-throughput data. H.Z., R.R.J. and J.J.G. wrote the manuscript.

## Competing interests

W.J.G. has affiliations with 10x Genomics (consultant). The other authors declare no competing interests.

## Additional information

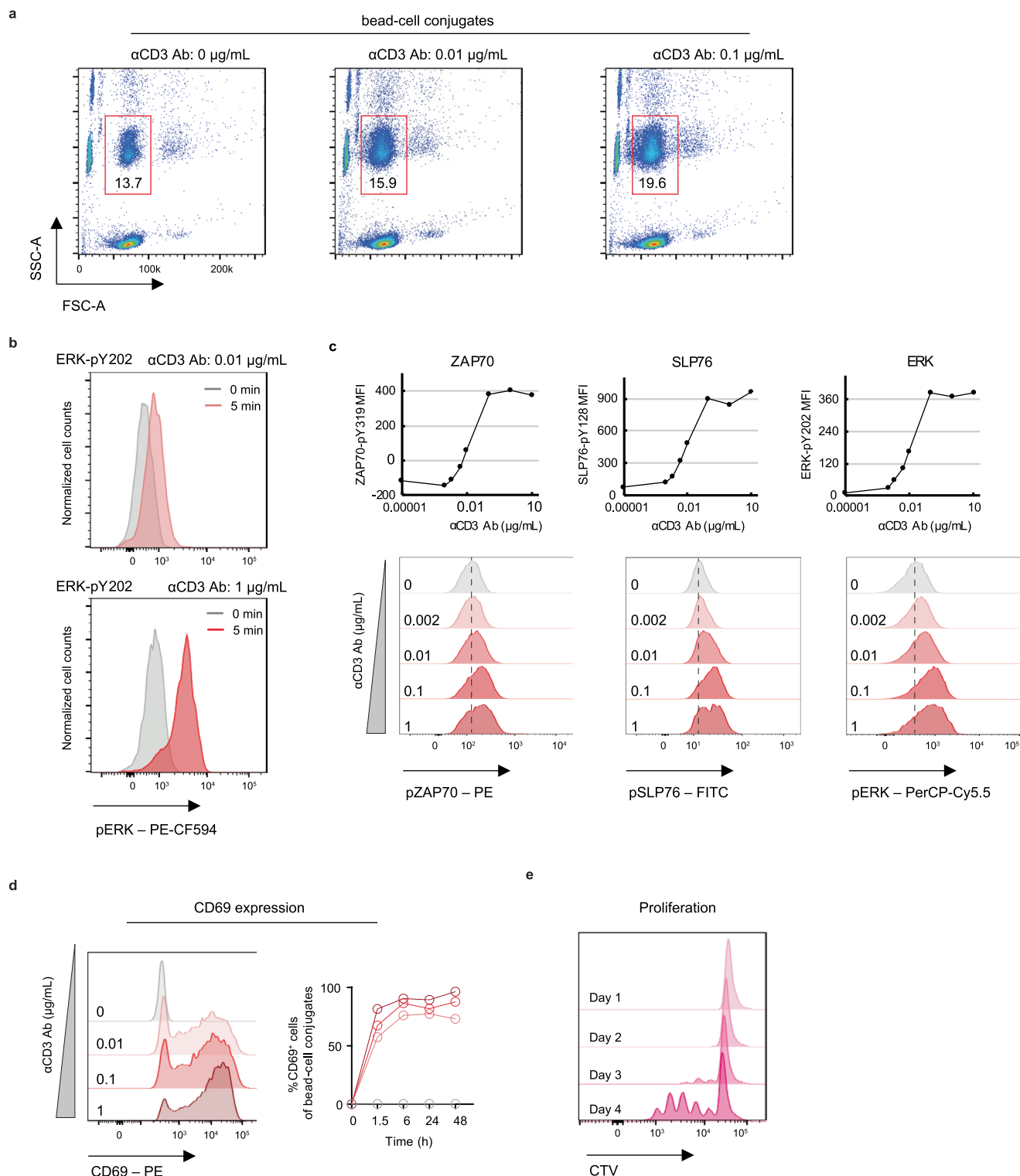
**Extended data** is available for this paper at <https://doi.org/10.1038/s41590-022-01369-x>.

**Supplementary information** The online version contains supplementary material available at <https://doi.org/10.1038/s41590-022-01369-x>.

**Correspondence and requests for materials** should be addressed to Jörg J. Goronzy.

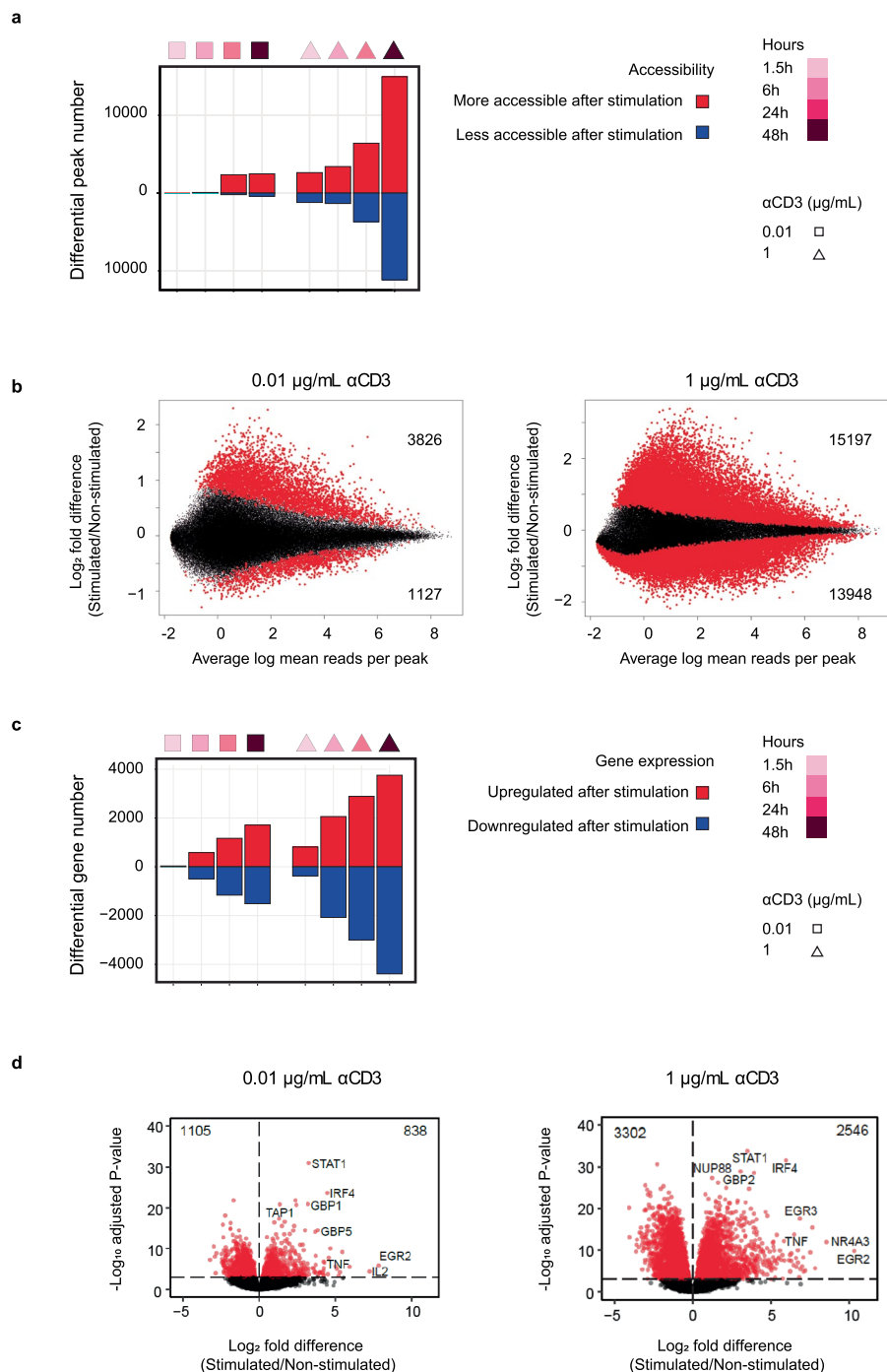
**Peer review information** *Nature Immunology* thanks Graham Pawelec, Benedict Seddon and Harinder Singh for their contribution to the peer review of this work. Primary Handling Editor: Laurie A. Dempsey, in collaboration with the *Nature Immunology* team. Peer reviewer reports are available.

**Reprints and permissions information** is available at [www.nature.com/reprints](http://www.nature.com/reprints).



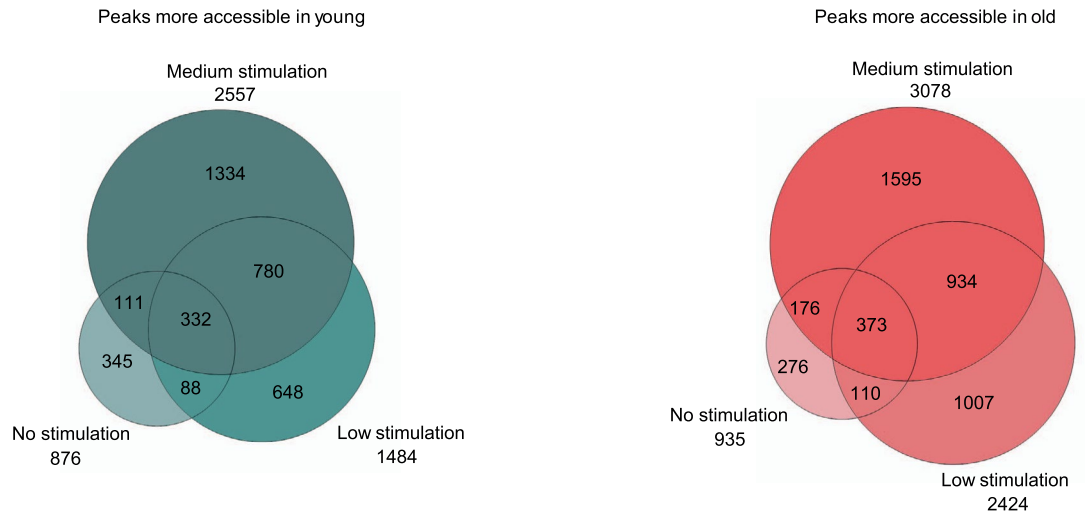
**Extended Data Fig. 1 | Related to Fig. 1: Titration of TCR stimulation.** Naive CD4<sup>+</sup> T cells were stimulated with polystyrene beads coated with indicated amounts of anti-CD3 Ab together with a constant amount of 1 μg mL<sup>-1</sup> anti-CD28. Bead-cell conjugates were gated and the percent of bound to total cells were determined. **b**, Histograms of phosphorylated ERK gated on bead-bound cells at 0 and 5 min stimulated with indicated amounts of anti-CD3. **c**, Mean fluorescence

intensity (MFI) of phosphorylated ZAP70, SLP76 and ERK was measured gated on bead-bound cells. **d**, Histogram of CD69 gated on bead-bound cells at 24 h of stimulation (left panel). Frequency of CD69<sup>+</sup> cells as percentage of total bead-bound cells from 0–48 h with indicated anti-CD3 concentrations (right panel). **e**, Cell Trace Violet dye dilution of naive CD4<sup>+</sup> T cells stimulated with 1 μg mL<sup>-1</sup> anti-CD3. Experiments shown are representative of three experiments.



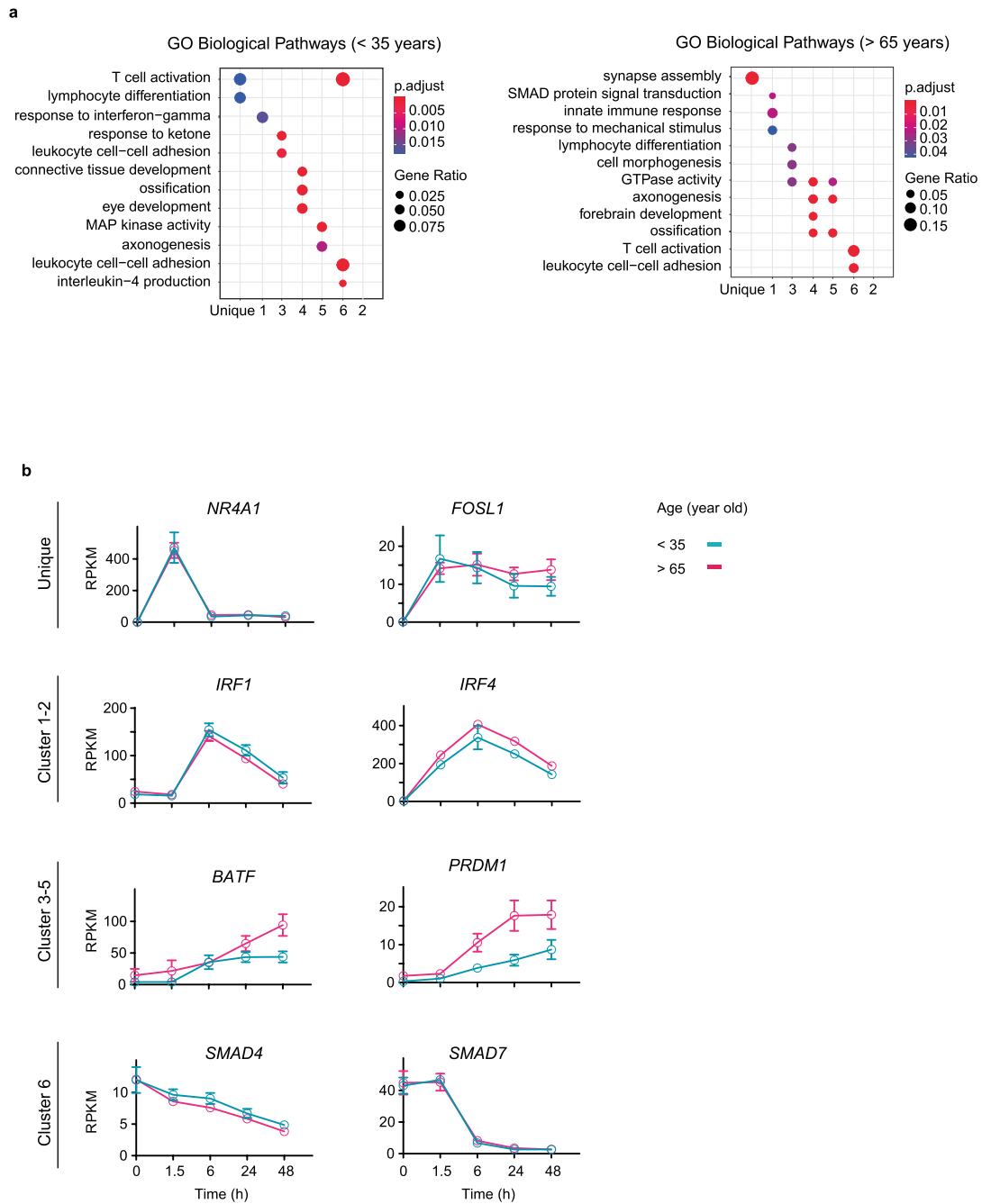
**Extended Data Fig. 2 | Related to Fig. 1a, b: Longitudinal epigenomic and transcriptomic changes induced by TCR stimulation.** Naive CD4<sup>+</sup> T cells from eight individuals were stimulated with 0.01 (low stimulation strength, square) or 1  $\mu$ g mL<sup>-1</sup> (medium strength, triangle) anti-CD3-coated beads and subjected to ATAC-seq and RNA-seq at indicated time points. **a**, Bar graphs show the number of peaks more or less accessible in activated cells compared to unstimulated cells at each time point. **b**, Differential peaks comparing unstimulated cells to either low (left) or high (right) TCR stimulation are plotted as average log<sub>2</sub> fold-

change (logFC) versus log<sub>2</sub> mean reads per peak. **c**, Bar graphs show the number of significantly up- or downregulated gene transcripts for each time point. **d**, Up- or downregulated gene transcripts in cells activated as indicated compared to unstimulated cells are shown as volcano plots of logFC versus significance levels. To illustrate similarities between stimulation conditions, few transcripts are labeled. Comparisons in **b, d** were done by two-sided robust empirical Bayes moderated statistical test; a Benjamini–Hochberg adjusted *P* value of 0.001 was used as cutoff.



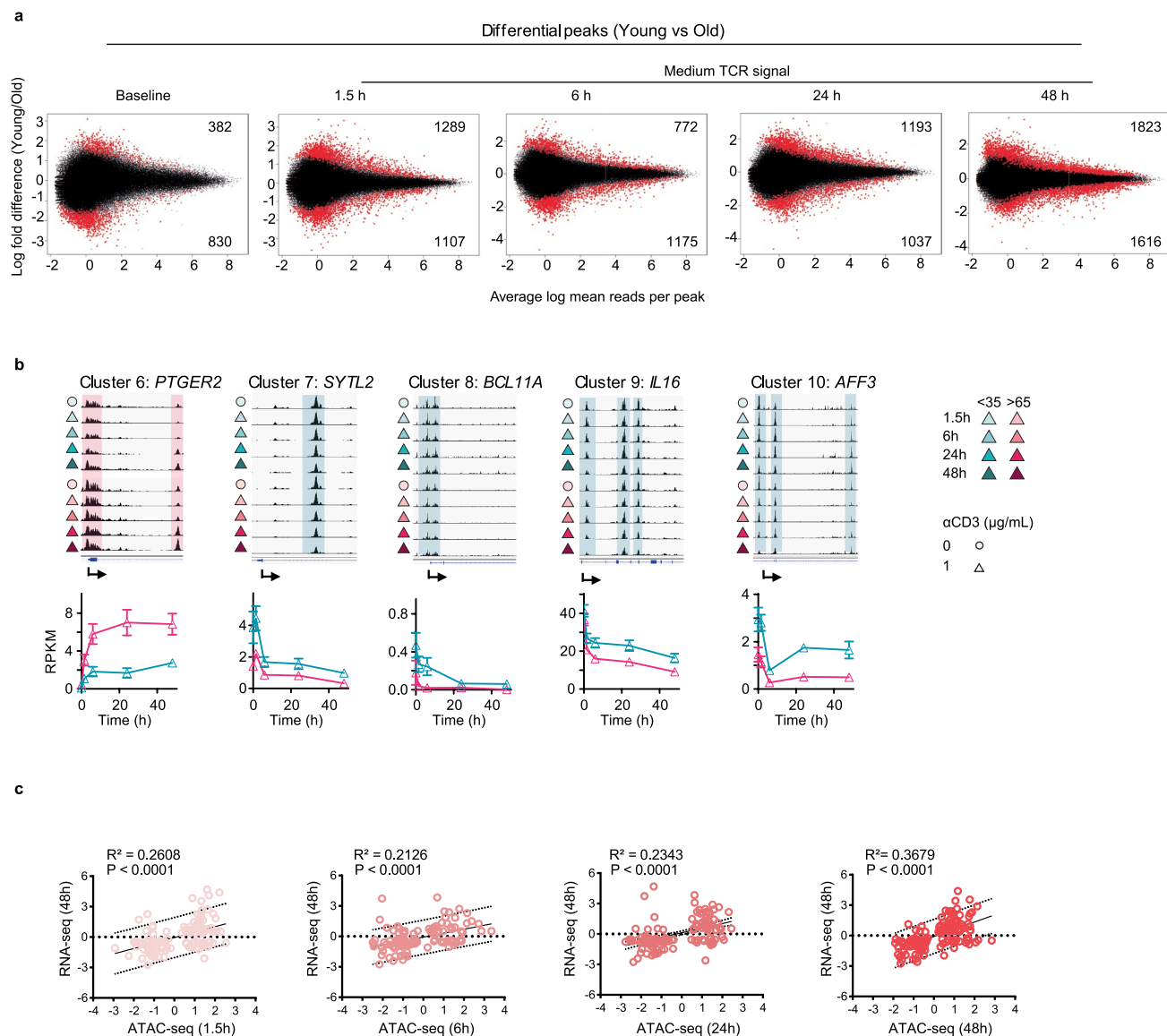
**Extended Data Fig. 3 | Related to Fig. 2: Higher intensity TCR stimulation amplifies age-associated chromatin accessibility differences seen at baseline or with low intensity stimulation.** Peak sets from ATAC-seq analysis of naive CD4<sup>+</sup> T cells from young (left) or old (right) adults were compared for each of the three conditions, unstimulated and after TCR stimulation with beads coated

with low and medium concentrations of anti-CD3. Comparisons were done by robust empirical Bayes moderated statistical test; a Benjamini–Hochberg adjusted *P* value of 0.05 was used as cutoff. Relationships between the three sets of differential peaks are shown as Venn diagrams.



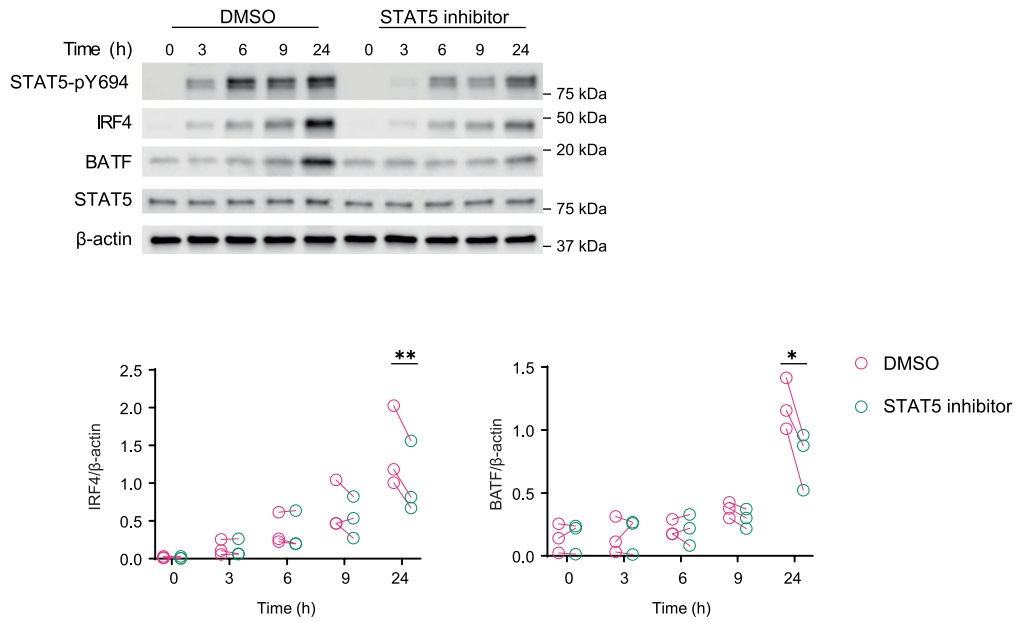
**Extended Data Fig. 4 | Related to Fig. 2c, d: Activation-induced temporal patterns of epigenetic changes in naive CD4<sup>+</sup> T cells from young and older adults.** **a**, Genes assigned to differentially accessible regulatory sites were examined for significant enrichment in biological pathways. Selected GO terms associated with the different temporal patterns in young (upper panel) and older

adults (lower panel) are shown. Comparisons were done by two-sided robust empirical Bayes moderated statistical test; a Benjamini–Hochberg adjusted *P* value of 0.05 was used as cutoff. **b**, Gene expression of indicated TFs shown as mean + s.e.m. *n* = 8 biologically independent samples.



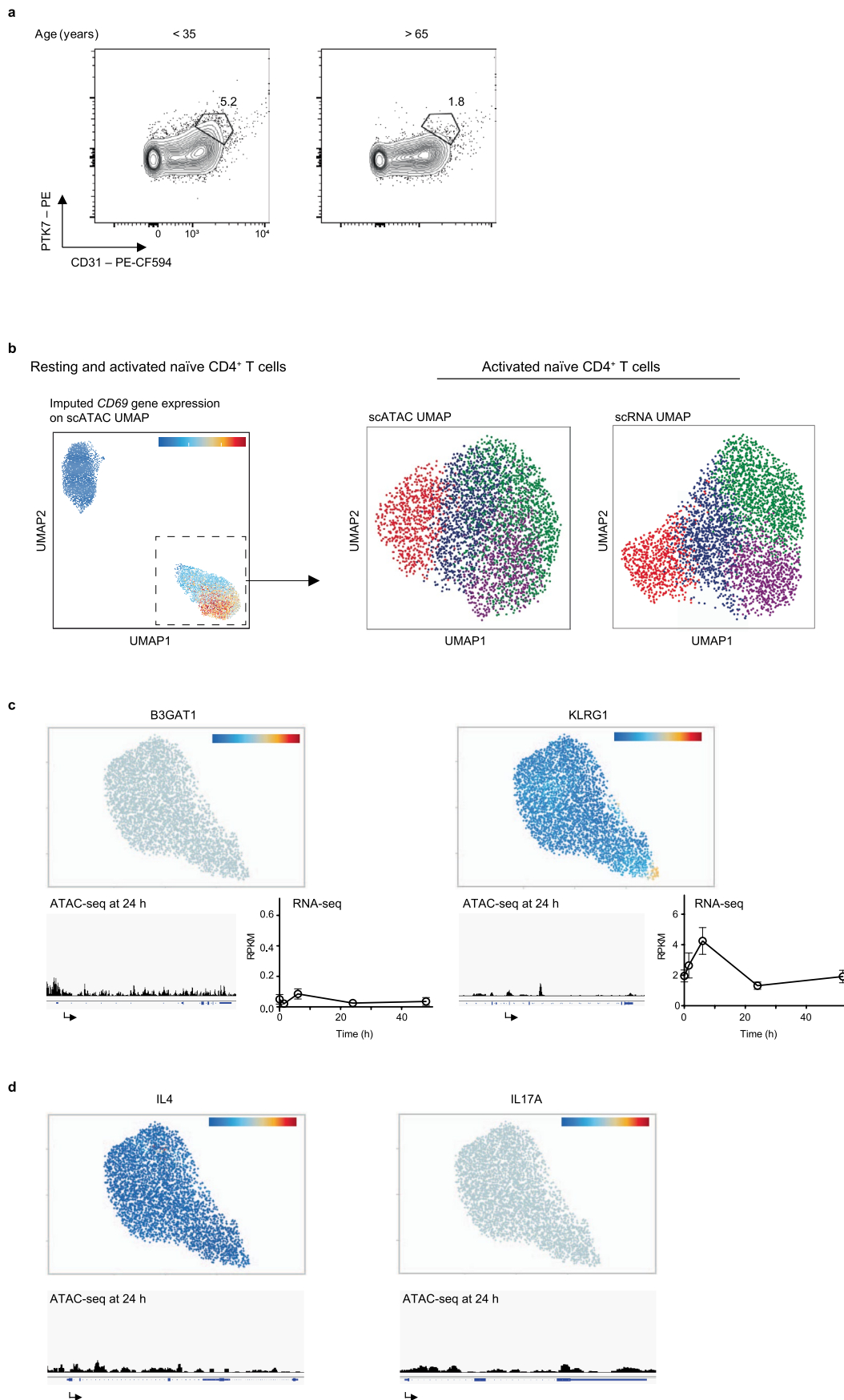
**Extended Data Fig. 5 | Related to Fig. 3c: Relationship between differential accessibility of regulatory regions and transcriptome. a**, Differential peaks between young and older individuals at indicated TCR stimulation conditions and time points are plotted as logFC versus log mean reads per peak. Comparisons were done by robust empirical Bayes moderated statistical test; a Benjamini–Hochberg adjusted  $P$  value of 0.05 was used as cutoff. **b**, Aggregate genome accessibility tracks (top panel) of representative sites of cluster 6–10 shown in the heat plot in Fig. 3c. Cyan-shaded areas indicate peaks that are more

open in young compared to older adults, magenta-shaded areas are more open in old. Transcript data from corresponding genes as determined by RNA-seq (lower panel) and shown as mean + s.e.m.  $n = 8$  biologically independent samples. **c**, LogFC difference of transcripts differentially expressed between young and older adults from 48-h RNA-seq data is plotted against logFC difference of differential peaks from ATAC-seq data annotated to the same gene at the indicated time point. Data are fitted with two-sided simple linear regression.  $P < 0.0001$ .



**Extended Data Fig. 6 | Related to Fig. 3h: Time course of TF expression after STAT5 inhibition.** Naive CD4<sup>+</sup> T cells from older adults were activated for 0–24 h with polystyrene beads coated with 1  $\mu\text{g mL}^{-1}$  anti-CD3 and anti-CD28 in the presence of DMSO solvent control or a STAT5 inhibitor. Representative western

blots (top panel). Summary data from 3 experiments showing band intensities of IRF4 and BATF relative to  $\beta$ -actin (bottom panel) and expressed as mean + s.e.m.  $n = 3$  biologically independent samples. Data were analyzed with two-sided paired t-test. \* $P < 0.05$  ( $p = 0.02$ ), \*\* $P < 0.01$  ( $p = 0.0094$ ).

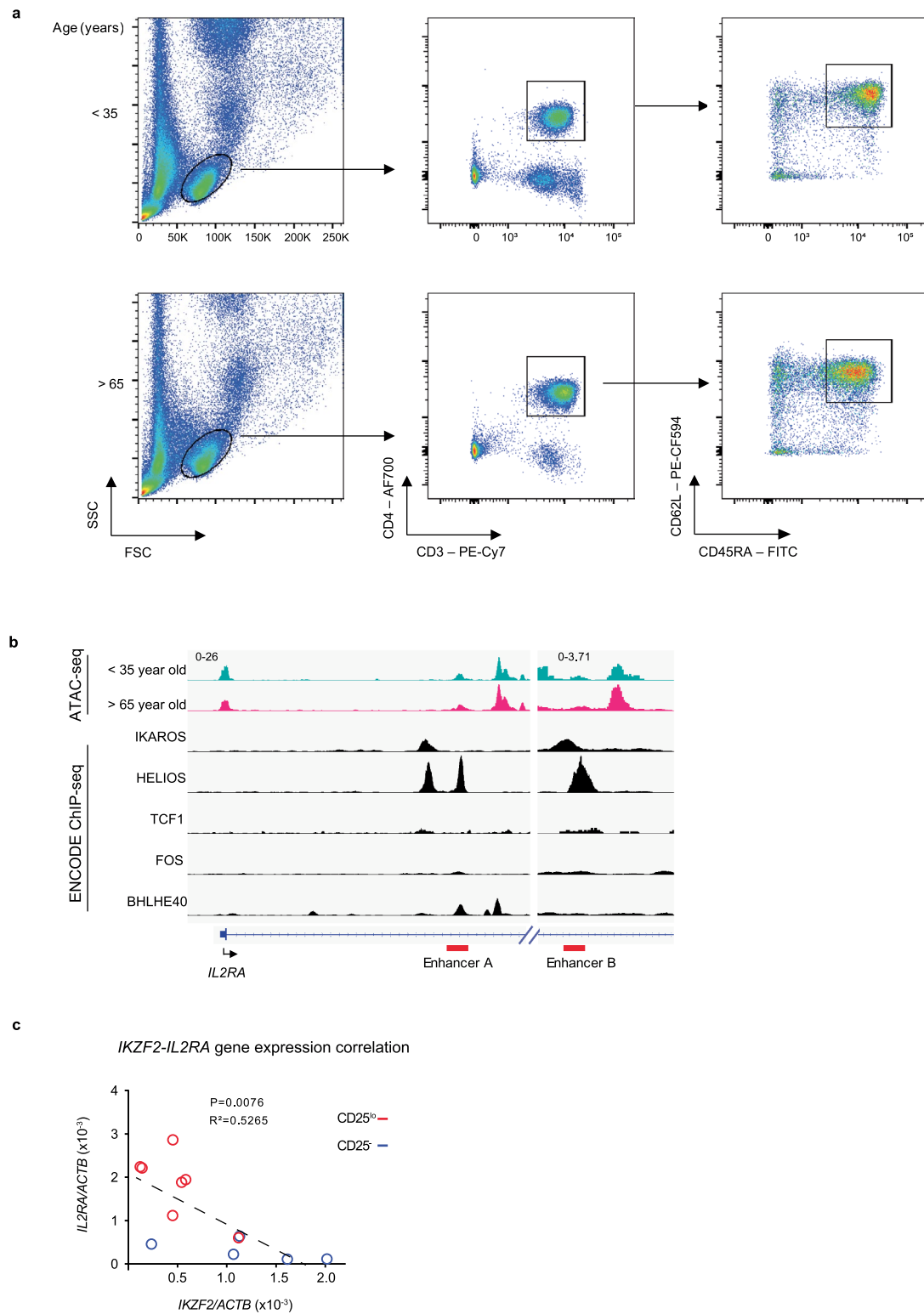


Extended Data Fig. 7 | See next page for caption.



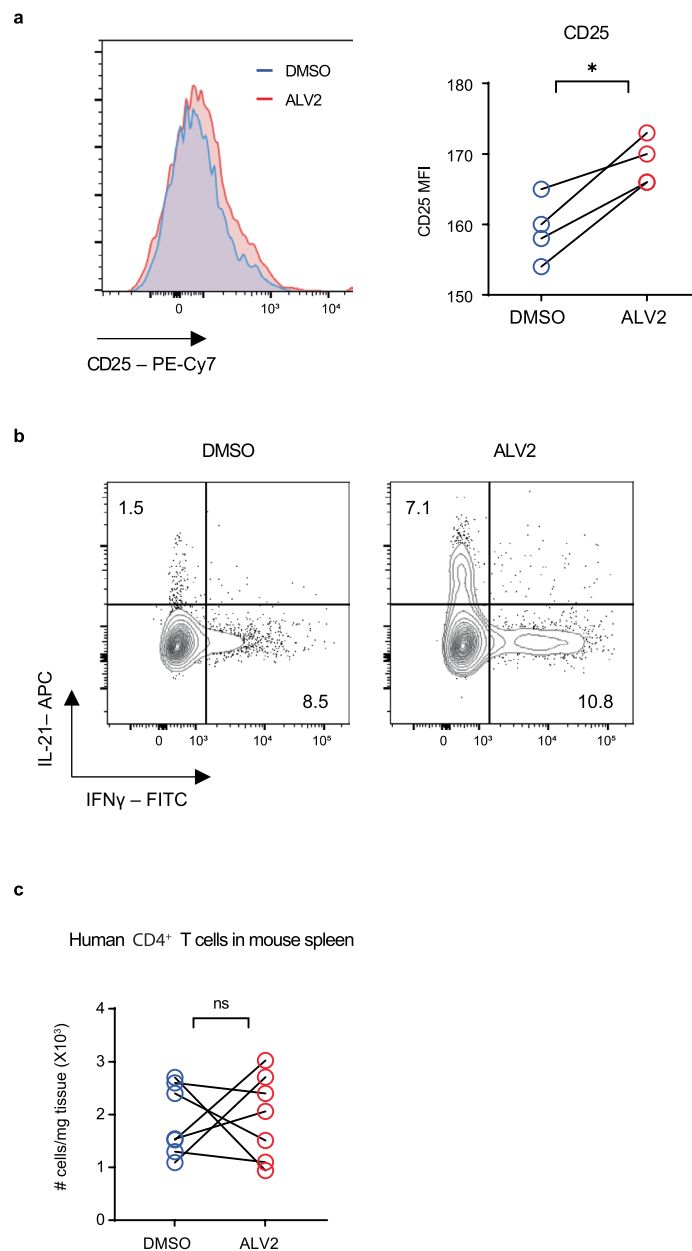
**Extended Data Fig. 7 | Related to Fig. 4: Single cell epigenetic and transcriptional analysis of naive CD4<sup>+</sup> T cell responses.** **a**, CD31 and PTK7 surface expression on naive CD4<sup>+</sup> T cells. **b**, Nuclei pooled from unstimulated and activated naive CD4<sup>+</sup> T cells were subjected to scATAC- and scRNA-seq. Imputed *CD69* gene expression is projected on the UMAP of scATAC-seq. Clusters of resting and activated cells were distinguished based on containing *CD69*-expressing cells (left panel). UMAP maps of scATAC-seq and scRNA-seq

data are shown for activated cells (right panels). **c**, *B3GAT1* and *KLRG1* gene expression were projected onto scMultiome UMAPs (top panel). Genome tracks of bulk ATAC-seq and gene expression in bulk RNA-seq expressed as mean + s.e.m. (bottom). n = 8 biologically independent samples. **d**, *IL4* and *IL17A* gene expression were projected onto scMultiome UMAPs (top panel). Genome tracks of bulk ATAC-seq at 24 h of TCR stimulation (bottom).



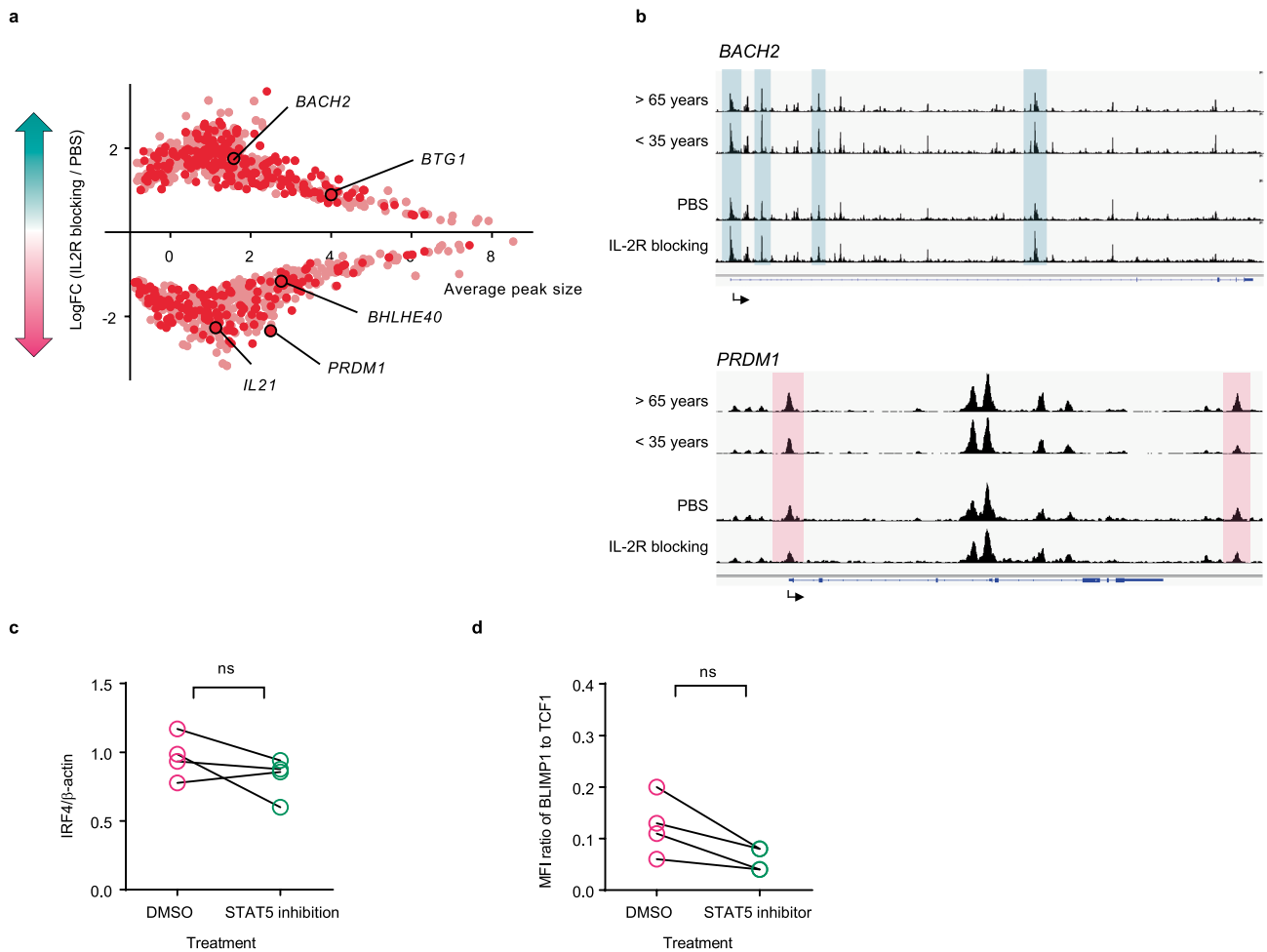
**Extended Data Fig. 8 | Related to Fig. 5b: TFs binding to *IL2RA* enhancers. a**, Gating strategy for naive CD4<sup>+</sup> T cells from PBMC of young and older individuals. **b**, ATAC-seq genome tracks of unstimulated naive CD4<sup>+</sup> T cells from young and older adults were aligned with ENCODE ChIP-seq genome tracks of indicated TFs

at *IL2RA* enhancer locus (see Fig. 5c). The location of enhancer A and enhancer B is indicated by red lines. **c**, *IKZF2* and *IL2RA* transcripts from sorted CD25<sup>lo</sup> and CD25<sup>+</sup> naive CD4<sup>+</sup> T cells from 7 donors. Data were fitted with two-sided simple linear regression.  $P=0.0076$ .



**Extended Data Fig. 9 | Related to Fig. 6: Naive CD4<sup>+</sup> T cell tissue infiltration after HELIOS degradation.** Naive CD4<sup>+</sup> T cells were treated with DMSO or 1  $\mu$ M ALV2 for 5 days. **a**, Histograms of CD25 gated on cells conjugated to beads after 4 h stimulation with 1  $\mu$ g mL<sup>-1</sup> anti-CD3 (left). Summary of CD25 MFI from four experiments (right).  $n = 4$  biologically independent samples. Data were analyzed with two-sided paired t-test.  $*P < 0.05$  ( $P = 0.01$ ). **b**, IL-21 and IFN $\gamma$

were stained after five days of activation with 5  $\mu$ g mL<sup>-1</sup> plate-coated anti-CD3 and 1  $\mu$ g mL<sup>-1</sup> anti-CD28. Data shown are representative of 4 (IFN $\gamma$ ) and 5 (IL21) experiments. **c**, Human CD4<sup>+</sup> T cells recovered from mouse spleen after 7-day engraftment.  $n = 7$  biologically independent samples. Data were analyzed with two-sided paired t-test.



**Extended Data Fig. 10 | Related to Fig. 7: Genome accessibility changes induced by IL-2 receptor blocking and effector TF expression induced by STAT5 inhibition.** **a**, LogFC of differential peaks between IL-2 receptor (IL-2R) blocking and PBS treatment are plotted against average peak size. Peaks that are also differentially accessible between young and older individuals are indicated in dark red. Comparisons were done by two-sided robust empirical Bayes moderated statistical test; a Benjamini-Hochberg adjusted  $P$  value of 0.05 was used as cutoff. **b**, Genome tracks of representative genes. Magenta-shaded areas indicate peaks that are more open in older adults and with PBS treatment;

cyan indicates peaks that are more open in young adults or with IL-2R blocking treatment of older adults. **c**, IRF4 protein expression were measured by Immuno blot in 48-h activated naive  $CD4^+$  T cells from four young adults with and without STAT5 inhibition.  $n = 4$  biologically independent samples. **d**, BLIMP1 and TCF1 expression was measured by flow cytometry in 5-day activated naive  $CD4^+$  T cells from four young adults. The MFI ratio of BLIMP1 to TCF1 was plotted.  $n = 4$  biologically independent samples. Data in **c**, **d** were analyzed with two-sided paired t-test.

## Reporting Summary

Nature Portfolio wishes to improve the reproducibility of the work that we publish. This form provides structure for consistency and transparency in reporting. For further information on Nature Portfolio policies, see our [Editorial Policies](#) and the [Editorial Policy Checklist](#).

### Statistics

For all statistical analyses, confirm that the following items are present in the figure legend, table legend, main text, or Methods section.

n/a Confirmed

- |                                     |                                     |  |
|-------------------------------------|-------------------------------------|--|
| <input type="checkbox"/>            | <input checked="" type="checkbox"/> | The exact sample size ( $n$ ) for each experimental group/condition, given as a discrete number and unit of measurement  |
| <input type="checkbox"/>            | <input checked="" type="checkbox"/> | A statement on whether measurements were taken from distinct samples or whether the same sample was measured repeatedly  |
| <input type="checkbox"/>            | <input checked="" type="checkbox"/> | The statistical test(s) used AND whether they are one- or two-sided<br><i>Only common tests should be described solely by name; describe more complex techniques in the Methods section.</i>   |
| <input checked="" type="checkbox"/> | <input type="checkbox"/>            | A description of all covariates tested   |
| <input type="checkbox"/>            | <input checked="" type="checkbox"/> | A description of any assumptions or corrections, such as tests of normality and adjustment for multiple comparisons  |
| <input type="checkbox"/>            | <input checked="" type="checkbox"/> | A full description of the statistical parameters including central tendency (e.g. means) or other basic estimates (e.g. regression coefficient) AND variation (e.g. standard deviation) or associated estimates of uncertainty (e.g. confidence intervals) |
| <input type="checkbox"/>            | <input checked="" type="checkbox"/> | For null hypothesis testing, the test statistic (e.g. $F$ , $t$ , $r$ ) with confidence intervals, effect sizes, degrees of freedom and $P$ value noted<br><i>Give <math>P</math> values as exact values whenever suitable.</i>                            |
| <input checked="" type="checkbox"/> | <input type="checkbox"/>            | For Bayesian analysis, information on the choice of priors and Markov chain Monte Carlo settings   |
| <input checked="" type="checkbox"/> | <input type="checkbox"/>            | For hierarchical and complex designs, identification of the appropriate level for tests and full reporting of outcomes   |
| <input checked="" type="checkbox"/> | <input type="checkbox"/>            | Estimates of effect sizes (e.g. Cohen's $d$ , Pearson's $r$ ), indicating how they were calculated   |

*Our web collection on [statistics for biologists](#) contains articles on many of the points above.*

### Software and code

Policy information about [availability of computer code](#)

Data collection BD FACSDiva (v8.0), QuantStudio Design and Analysis (v2.5).

Data analysis R(v4.0), R-libraries (Rsubread (1.28.1), edgeR (3.38.4), limma (3.41.5), DESeq2 (1.30.1), cqn (1.36.0), cluster (2.4.), TCseq (1.21.0), ArchR (1.0.1), ChromVar (1.12.0), macs(v2.1.1), bowtie(v2.2.4), samtools(v1.3), bedtools(v2.26.0), homer(v4.8), cellranger-arc(v1.0.1), Graphpad prism (v8.0), FlowJo (v9.0).

For manuscripts utilizing custom algorithms or software that are central to the research but not yet described in published literature, software must be made available to editors and reviewers. We strongly encourage code deposition in a community repository (e.g. GitHub). See the Nature Portfolio [guidelines for submitting code & software](#) for further information.

### Data

Policy information about [availability of data](#)

All manuscripts must include a [data availability statement](#). This statement should provide the following information, where applicable:

- Accession codes, unique identifiers, or web links for publicly available datasets
- A description of any restrictions on data availability
- For clinical datasets or third party data, please ensure that the statement adheres to our [policy](#)

GRCh37 genome, GSE22886, GSE8685, R-HSA-8949275 and R-HSA-2559584 from MSigDB were used in this study. Raw sequencing data have been deposited in SRA with the BioProject accession # PRJNA757466. Raw experimental data will be provided by the corresponding author upon request.

## Field-specific reporting

Please select the one below that is the best fit for your research. If you are not sure, read the appropriate sections before making your selection.

Life sciences  Behavioural & social sciences  Ecological, evolutionary & environmental sciences

For a reference copy of the document with all sections, see [nature.com/documents/nr-reporting-summary-flat.pdf](https://www.nature.com/documents/nr-reporting-summary-flat.pdf)

## Life sciences study design

All studies must disclose on these points even when the disclosure is negative.

Sample size	Sample sizes to identify differences between young and older adults were chosen to ensure 80% power with a level of significance of 5% when the difference in their means would be 1.5 standard deviation ( $n > 10$ ). For intervention experiments, we used a sample size of 3-6.
Data exclusions	No data were excluded.
Replication	All experiments have been replicated at least once and results were successfully reproduced.
Randomization	The general study design was to compare individuals less than 35 years old and older than 65 years, thus the individuals selected for the study cannot be randomized.
Blinding	Investigators were not blinded.

## Reporting for specific materials, systems and methods

We require information from authors about some types of materials, experimental systems and methods used in many studies. Here, indicate whether each material, system or method listed is relevant to your study. If you are not sure if a list item applies to your research, read the appropriate section before selecting a response.

### Materials & experimental systems

n/a	Involved in the study
<input type="checkbox"/>	<input checked="" type="checkbox"/> Antibodies
<input type="checkbox"/>	<input checked="" type="checkbox"/> Eukaryotic cell lines
<input checked="" type="checkbox"/>	<input type="checkbox"/> Palaeontology and archaeology
<input type="checkbox"/>	<input checked="" type="checkbox"/> Animals and other organisms
<input type="checkbox"/>	<input checked="" type="checkbox"/> Human research participants
<input checked="" type="checkbox"/>	<input type="checkbox"/> Clinical data
<input checked="" type="checkbox"/>	<input type="checkbox"/> Dual use research of concern

### Methods

n/a	Involved in the study
<input checked="" type="checkbox"/>	<input type="checkbox"/> ChIP-seq
<input type="checkbox"/>	<input checked="" type="checkbox"/> Flow cytometry
<input checked="" type="checkbox"/>	<input type="checkbox"/> MRI-based neuroimaging

## Antibodies

### Antibodies used

Anti-human CD69 (BioLegend, Cat: 310905, Clone: FN50), Anti-human CD25 (BioLegend, Cat:302618, Clone: BC96, Lot: B261579), Anti-human CD25 PE (BioLegend, Cat: 302605, Clone: BC96), Anti-human CD3 (BD, Cat: 557851, Clone: SK7, Lot: 9079612), Anti-human CD4 (BioLegend, Cat: 344622, Clone: SK3, Lot: B304453), Anti-human CD45RA (BD, Cat: 555488, Clone: HI100, Lot: 0016333), Anti-human CD62L (BD, Cat: 562301, Clone: Dreg-56, Lot: 9315723), Anti-ZAP70 pY319 (BD, Cat: 557817, Clone: 17A/P-ZAP70, Lot: 4041999), Anti-SLP76 pY128 (BD, Cat: 558439, Clone: J141-668.36.58, Lot: 7104554), Anti-ERK pT202 (BD, Cat: 562644, Clone: 20A, Lot: 8283532), Anti-TCF1 PE (BioLegend, Cat: 65520725, Clone: 7F11A10, Lot: B291681), Anti-human BLIMP1 (R&D systems, Cat: IC36081A, Clone: 646702, Lot: AEPP0119091), Anti-IRF4 (Cell Signaling, Cat: 4964, polyclonal, Lot: 4), Anti-BHLHE40 (Novus Bio, Cat: NB100-1800, polyclonal, Lot: E-2), Anti- $\beta$ -actin (Cell Signaling, Cat: 4970, Clone: 13E5, Lot: 15), Anti-ERK pT202 (Cell Signaling, Cat: 9101, polyclonal, Lot: 30), Anti-LAT pY132 (Invitrogen, Cat: 44-224, polyclonal, Lot: SF235298), Anti-STAT5 pY694 (Cell Signaling, Cat: 9351, polyclonal, Lot: 9), Anti-HELIOS (Cell Signaling, Cat: 42427, Clone: D8W4X, Lot: 1), Anti-human CD25 (BioLegend, Cat: 302602, Clone: BC96, Lot: B278786), Anti-human CD122 (BioLegend, Cat: 339002, Clone: TU27, Lot: B205250), Anti-human PTK7 (Miltenyi, Cat: 130-122-967, Clone CCK-4), Anti-human CD31 (BioLegend, Cat: 303129, Clone: WM59), Anti-human CD38 (BioLegend, Cat: 356613, Clone: HB-7), Anti-human IL-21 (BioLegend, Cat: 513005, Clone: 3A3-N2), Anti-human IFN $\gamma$  (BioLegend, Cat: 502505, Clone: 4S.B3), Anti-human STAT5 (Cell Signaling, Cat: 94205T, Clone: D2O6Y). Surface staining antibodies were used with 1:50 dilution. Intracellular staining antibodies were used at 1:20 dilution. Immunoblot antibodies were used at 1:1000 dilution.

### Validation

All antibodies were purchased from established vendors with strict quality control assurances. Please refer to the data sheet from the vendor's website for technical info.

## Eukaryotic cell lines

Policy information about [cell lines](#)

Cell line source(s)	HEK293T, ATCC, CRL-11268
Authentication	Cell lines were not authenticated.
Mycoplasma contamination	Cell lines were not tested for contamination.
Commonly misidentified lines (See <a href="#">ICLAC</a> register)	Commonly misidentified cell lines were not used in the study.

## Animals and other organisms

Policy information about [studies involving animals](#); [ARRIVE guidelines](#) recommended for reporting animal research

Laboratory animals	NOD.Cg-Prkdcscid Il2rgtm1Wjl/SzJ (NSG) mice were maintained under pathogen-free conditions on a 12/12 h light dark cycle at 20-22 C with free access to water and food. Animal housing facilities were monitored for infection with specific pathogens every six weeks and health status of all animals was checked on a daily basis. Both genders of mice of 8-12 weeks of age were included for experiments.
Wild animals	The study did not involve wild animals.
Field-collected samples	The study did not involve field-collected samples.
Ethics oversight	Mayo Clinic Institutional Animal Care and Use Committee

Note that full information on the approval of the study protocol must also be provided in the manuscript.

## Human research participants

Policy information about [studies involving human research participants](#)

Population characteristics	123 de-identified donors were obtained from blood bank with 66 aged from 20-35 and 57 aged over 65 years. 16 participants were recruited for sequencing experiments including 9 male and 7 females aged from 25-81 years. Covariate-relevant population characteristics of the recruited human participants are provided in supplementary table 1.
Recruitment	For sequencing, 16 individuals were recruited who did not have an acute or active chronic disease or a history of cancer or autoimmune diseases. Chronic diseases such as hypertension were permitted if controlled by medication. The individuals were recruited by flyers and scheduled by email or phone call. The only selection criteria of participants besides the above stated health conditions were their age either less than 35 years old or greater than 65 years old.
Ethics oversight	Institutional Review Board (IRB) Stanford; Institutional Review Board (IRB) Mayo Clinic.

Note that full information on the approval of the study protocol must also be provided in the manuscript.

## Flow Cytometry

### Plots

Confirm that:

- The axis labels state the marker and fluorochrome used (e.g. CD4-FITC).
- The axis scales are clearly visible. Include numbers along axes only for bottom left plot of group (a 'group' is an analysis of identical markers).
- All plots are contour plots with outliers or pseudocolor plots.
- A numerical value for number of cells or percentage (with statistics) is provided.

### Methodology

Sample preparation	PBMC were Ficoll-isolated from buffy coats, LRS cones or whole blood. Naïve CD4+ T cells were isolated by negative selection.
Instrument	BD LSR Fortessa
Software	FlowJo v9.0
Cell population abundance	The purity of naïve CD4+ T cells was at least 95%.

Gating strategy

FSC-A/SSC-A was used to gate lymphocytes. FSC-H/FSC-W was used to select single cells. Live cells were gated as Aqua negative. CD3 was used to gate T cells. CD4, CD45RA and CD62L were used to gate naïve CD4+ T cells.

Tick this box to confirm that a figure exemplifying the gating strategy is provided in the Supplementary Information.